

**The CU Airborne
MAX-DOAS
instrument**

S. Baidar et al.

**The CU Airborne MAX-DOAS instrument:
ground based validation, and vertical
profiling of aerosol extinction and
trace gases**

**S. Baidar^{1,2}, H. Oetjen^{1,*}, S. Coburn¹, B. Dix¹, I. Ortega¹, R. Sinreich¹, and
R. Volkamer^{1,2}**

¹Department of Chemistry and Biochemistry, University of Colorado, Boulder, CO, 80309, USA

²Cooperative Institute for Research in Environmental Sciences (CIRES), Boulder, CO,
80309, USA

*now at: Jet Propulsion Laboratory (JPL), Pasadena, CA 91109, USA

Received: 2 August 2012 – Accepted: 13 September 2012 – Published: 26 September 2012

Correspondence to: R. Volkamer (rainer.volkamer@colorado.edu)

Published by Copernicus Publications on behalf of the European Geosciences Union.

Title Page

Abstract

Introduction

Conclusions

References

Tables

Figures

◀

▶

◀

▶

Back

Close

Full Screen / Esc

Printer-friendly Version

Interactive Discussion



Abstract

The University of Colorado Airborne Multi Axis Differential Optical Absorption Spectroscopy (CU AMAX-DOAS) instrument uses solar stray light remote sensing to detect and quantify multiple trace gases, including nitrogen dioxide (NO₂), glyoxal (CHOCHO), formaldehyde (HCHO), water vapor (H₂O), nitrous acid (HONO), iodine monoxide (IO), bromine monoxide (BrO), and oxygen dimers (O₄) at multiple wavelengths (360 nm, 477 nm, 577 nm and 632 nm) simultaneously, and sensitively in the open atmosphere. The instrument is unique, in that it presents the first systematic implementation of MAX-DOAS on research aircraft, i.e. (1) includes measurements of solar stray light photons from nadir, zenith, and multiple elevation angles forward and below the plane by the same spectrometer/detector system, and (2) features a motion compensation system that decouples the telescope field of view (FOV) from aircraft movements in real-time (< 0.35° accuracy). Sets of solar stray light spectra collected from nadir to zenith scans provide some vertical profile information within 2 km above and below the aircraft altitude, and the vertical column density (VCD) below the aircraft is measured in nadir view. Maximum information about vertical profiles is derived simultaneously for trace gas concentrations and aerosol extinction coefficients over similar spatial scales and with a vertical resolution of typically 250 m during aircraft ascent/descent.

The instrument is described, and data from flights over California during the CalNex and CARES air quality field campaigns is presented. Horizontal distributions of NO₂ VCDs (below the aircraft) maps are sampled with typically 1 km resolution, and show good agreement with two ground based CU MAX-DOAS instruments (slope 0.95 ± 0.09 , $R^2 = 0.86$). As a case study vertical profiles of NO₂, CHOCHO, HCHO, and H₂O mixing ratios and aerosol extinction coefficients, ϵ , at 477 nm calculated from O₄ measurements from a low approach at Brackett airfield inside the South Coast Air Basin (SCAB) are presented. These profiles contain ~ 12 degrees of freedom (DOF) over a 3.5 km altitude range, independent of signal-to-noise at which the trace gas is detected. The boundary layer NO₂ concentration, and the integral aerosol extinction over

AMTD

5, 7243–7292, 2012

The CU Airborne MAX-DOAS instrument

S. Baidar et al.

Title Page

Abstract

Introduction

Conclusions

References

Tables

Figures

◀

▶

◀

▶

Back

Close

Full Screen / Esc

Printer-friendly Version

Interactive Discussion



**The CU Airborne
MAX-DOAS
instrument**S. Baidar et al.

[Title Page](#)[Abstract](#)[Introduction](#)[Conclusions](#)[References](#)[Tables](#)[Figures](#)[⏪](#)[⏩](#)[◀](#)[▶](#)[Back](#)[Close](#)[Full Screen / Esc](#)[Printer-friendly Version](#)[Interactive Discussion](#)

telescopes, pointing at fixed EAs. A boundary layer NO₂ profile was obtained by Dix et al. (2009) using multiple lines of sight (LOS) and a descent of an aircraft. Prados-Roman et al. (2011) used only one LOS parallel to the plane and the aircraft descent to retrieve vertical profiles of bromine oxide, BrO in the Arctic. Most recently, a limb scanning airborne DOAS instrument was developed at Belgium Institute for Space Aeronomy (BIRA) to obtain vertical distribution of trace gases like NO₂ (Merlaud et al., 2011). Most airborne DOAS instruments use either a single or multiple fixed LOS and use a spectrum collected from the same EA as the reference spectrum for DOAS analysis. The DOAS technique yields relative differences in absorber amounts between a measured spectrum and a reference spectrum. These instruments also lack control of the viewing geometry of the telescope during the flight. Pitch and roll information from the aircraft is used during post-processing to calculate the true viewing angle at the time of measurement during the flight. This often leads to an average EA assigned to a measurement and results in a larger uncertainty since MAX-DOAS instruments rely on exactly assigned viewing angles to retrieve vertical profile information of trace gases.

Here, we describe the University of Colorado Airborne MAX-DOAS (CU AMAX-DOAS) instrument, which to our knowledge presents the first true MAX-DOAS implementation from research aircraft. The CU AMAX-DOAS instrument has the capability to access zenith, nadir and limb viewing geometry by means of a single, rotatable prism telescope which is coupled to a motion compensation system. The motion compensation system includes angle sensors to measure pitch and roll angles of the aircraft and feedback loop to correct for it in real-time the pointing angle of the telescope to maintain a constant EA during spectra acquisition in flight. This isolates the telescope from aircraft movements, and enables us to systematically probe the atmosphere with desired sets of EAs to retrieve vertical profiles of trace gases and aerosol extinction simultaneously, and with the highest possible information content. The use of a single telescope to collect spectra from zenith, and other EAs (nadir, and forward of the plane) further enables the zenith spectra to be used as the Fraunhofer reference spectrum in

The CU Airborne MAX-DOAS instrument

S. Baidar et al.

Title Page

Abstract

Introduction

Conclusions

References

Tables

Figures

⏪

⏩

◀

▶

Back

Close

Full Screen / Esc

Printer-friendly Version

Interactive Discussion



the DOAS analysis. Zenith spectra usually contain the least amount of tropospheric absorbers, and the ability to record zenith spectra close in time to other EA spectra assures that absorbers above the plane are characterized with minimum difference in radiation fields, and makes the instrument inherently more sensitive to absorbers near and below the aircraft altitude (Volkamer et al., 2009a).

The CU AMAX-DOAS instrument was successfully deployed from 19 May–19 July 2010 as part of two air quality studies in California, namely the California Research at the Nexus of Air Quality and Climate Change (CalNex) (see overview paper by Ryerson et al., 2012) and the Carbonaceous Aerosols and Radiative Effects Study (CARES) (see overview paper by Zaveri et al., 2012). A total of 52 research flights were performed during this deployment and here we focus on results from one flight on 16 July 2010 to describe the technique, and characterize instrument performance. In Sect. 2 the CU AMAX-DOAS instrument is described, and the instrument configuration is introduced. Section 3 describes the DOAS analysis procedures, radiative transfer model (RTM) calculations, and algorithms to retrieve VCDs and vertical profiles of the trace gas concentrations and aerosol extinction coefficients. Section 4 demonstrates the capability of the new instrument. As a case study, vertical profiles of NO₂, CHOCHO, HCHO, H₂O and aerosol extinction coefficients at 477 nm are retrieved from a low approach at Brackett airfield in the South Coast Air Basin (SCAB). Finally, as a validation, CU AMAX-DOAS NO₂ VCDs are compared with VCDs measured by two CU ground based MAX-DOAS instruments that were regularly over-passed during flights; the boundary layer NO₂ concentration retrieved from the vertical profile is compared to a ground-based in-situ sensor concentration, and the integral aerosol extinction over height, i.e. AOD is compared with data from an AERONET station.

2 The CU AMAX-DOAS Instrument

The CU-AMAX-DOAS instrument collects spectra of scattered sunlight between 330 and 720 nm at different EAs. The scattered sunlight spectra are analyzed for the

The CU Airborne MAX-DOAS instrument

S. Baidar et al.

Title Page

Abstract

Introduction

Conclusions

References

Tables

Figures

◀

▶

◀

▶

Back

Close

Full Screen / Esc

Printer-friendly Version

Interactive Discussion



presence of absorbers, using the DOAS method (Platt and Stutz, 2008), like NO₂, CHOCHO, HCHO, H₂O, HONO, IO, BrO, O₄. NO₂, CHOCHO, HCHO, H₂O and O₄ data will exemplarily be presented in this paper. The instrument consists of a telescope pylon mounted on the outside of a window plate on a NOAA Twin Otter Remote Sensing research aircraft. The collected photons are transferred via optical fibers to two synchronized spectrometer-detector systems that are housed inside the aircraft fuselage. An optical fiber switch box is placed in between the light sources (telescopes and Hg calibration lamp) and the spectrometer-detector systems to select between different light sources at a given time. The Hg calibration lamp is used to characterize the optical resolution of the spectrometer-detector systems. The instrumental setup is shown in Fig. 2.

2.1 Telescope system

The telescope is designed for high light throughput and a very narrow vertical field of view (0.3° × 5.89°). It comprises a 1/2'' rotating prism, a 1/2'' lens tube with a 1/2'' f/4 lens and a stepper motor. All the telescope components are housed in a telescope pylon, an aluminum housing with quartz windows, which is mounted on the outside of a window plate on a NOAA Twin Otter research aircraft. The rotating prism is installed with 0° EA parallel to the aircraft heading and is driven by a stepper motor with an internal encoder to rotate vertically. The prism is capable of making a complete 360° rotation and hence allows characterization of the air masses above, below and in front of the aircraft using the same telescope. Viewing directions behind the aircraft are not accessible due to the structural design of the pylon including the placement of viewing ports. An additional telescope with a fixed EA is therefore present in the pylon to reach some of the inaccessible viewing geometries of the rotating prism. This telescope was rarely used during CalNex and CARES campaigns and data from this telescope is not presented in this paper. The viewing ports on the pylon are heated to prevent formation of ice at higher altitudes. The pylon also includes two webcams; a downward and a forward looking one, to capture atmospheric conditions during the flight. The

light collected by the rotatable prism is focused via a lens tube onto a 12 m long fiber bundle consisting of $72 \times 145 \mu\text{m}$ fibers. The fiber bundle is configured into two rows of 36 fibers at the telescope end and a circular arrangement at the other. The ends of the fibers away from the telescope are connected to a custom-made optical fiber switch box.

2.2 Optical fiber switch box

The optical fiber switch box is used to select between different incoming light sources. It consists of a translational stage mounted to a stepper motor linear actuator. The fibers from the telescopes and Hg calibration lamp are connected to one end of the box. A 10 m long 1.7 mm diameter silica mono-fiber, which is used as a mixing fiber to minimize polarization effects, is mounted on the translational stage opposite the incoming fibers from the light sources. The motor of the linear actuator drives the platform to place the mono-fiber directly in front of the desired fiber with the incoming light at a given time. The other end of the mono-fiber is connected to a bifurcated fiber bundle ($72 \times 145 \mu\text{m}$) to deliver light to two spectrometers simultaneously. The bifurcated ends are aligned in a single row of 36 fibers to connect to the spectrograph entrance slits.

2.3 Spectrometer and detector system

Two spectrometers and their respective detectors are housed in a standard 19" aluminum instrument rack ($19'' \times 22'' \times 10 \frac{1}{2}''$) with modifications to the bottom and top plates for added stability. The spectrometers are Princeton Instrument Acton SP2150 Imaging Czerny-Turner spectrometers with PIXIS 400 back illuminated CCD detectors. The first spectrometer (later referred to as the O_4 spectrometer) is equipped with a $500 \text{ grooves mm}^{-1}$ grating, blazed at 330 nm. It covers 350–720 nm and is used to measure all four major O_4 bands at 360, 477, 577 and 632 nm. The second spectrometer (later referred to as trace gas (TG) spectrometer) covers a wavelength range from 330–470 nm with a custom $1000 \text{ grooves mm}^{-1}$ (250 nm blaze wavelength) grating. It

The CU Airborne MAX-DOAS instrument

S. Baidar et al.

Title Page

Abstract

Introduction

Conclusions

References

Tables

Figures

◀

▶

◀

▶

Back

Close

Full Screen / Esc

Printer-friendly Version

Interactive Discussion



is used to measure all other trace gases. The optical resolution of the O₄ and TG spectrometers were ~2.2 and ~0.7 nm, respectively, inferred from the full-width at half-maximum (FWHM) of a representative Hg line. The CCDs are cooled to -30 °C to reduce dark current. The temperatures of the spectrometers are actively controlled with heaters while the instrument rack box temperature is actively cooled using peltier cooling units assuring a constant temperature over a range of varying ambient temperatures. Please refer to Coburn et al. (2011) for additional information on temperature stability, data acquisition and electronic and dark current correction for a comparable instrument. To reduce stray light and higher order diffraction in the TG spectrometer, two filters, a BG3 and a BG38, were placed immediately after the shutter.

2.4 Motion compensation system

The motion compensation system is used to correct the viewing geometry of the telescope for the aircraft pitch and roll effects during the flight. It consists of a PC104 computer connected to the prism motor and two angle sensors, a Systron Donner Inertial MMQ-G, and an electronic clinometer. The MMQ-G is a small robust Global Positioning System (GPS) based Inertial Navigation System (INS). It provides accurate 3-dimensional position, time, velocity, and attitude. It is primarily used to measure the pitch and roll angles of the aircraft for our application and has an angle accuracy of 5 mrad (~0.29°). The information from the sensor is processed by custom LabVIEW software into the coordinate system along the horizon. It is then used to drive the stepper motor of the prism to a new position such that it corrects for the aircraft's movement and keeps the telescope at the desired EA. The software has capability for 100 Hz loop rate, and was typically operated at 10 Hz. The stepper motor has a precision of 0.01° but is limited by the resolution of the internal encoder (0.2°) to precisely read back the position of the motor. The MMQ-G, clinometer and the telescope prism are mounted on planes parallel to the ground such that the elevation angle of the telescope and the pitch of the aircraft read zero simultaneously. The clinometer is used as a backup during flights for situations when the GPS signal required for the MMQ-G is lost. The

The CU Airborne MAX-DOAS instrument

S. Baidar et al.

Title Page

Abstract

Introduction

Conclusions

References

Tables

Figures



Back

Close

Full Screen / Esc

Printer-friendly Version

Interactive Discussion



theoretical angle accuracy of the motion compensation system is 0.35° considering the MMQ-G accuracy of $\sim 0.29^\circ$ (1σ) and motor internal encoder resolution of 0.2° . The system is configured to reset the motor when it does not reach a given position within a desired tolerance level by a fixed time interval. The same motion compensation system has also been integrated as part of another telescope pylon designed for adaptation of the CU AMAX-DOAS instrument aboard the NSF/NCAR GV HIAPER aircraft.

2.5 Performance of the motion compensation system

Figure 3 shows the performance of the system during research flights aboard the GV HIAPER and Twin Otter aircrafts. GV HIAPER flights provide an excellent opportunity to test the system as the aircraft pitch and roll angles measured by the aircraft avionics system during the flight are recorded, while avionics data for the Twin Otter flights are not available. The histogram of differences in aircraft pitch angle recorded at 1 Hz frequency measured by NSF/NCAR GV HIAPER aircraft avionics and our MMQ-G recording during a research flight (~ 8 h) on 24 February 2012 is plotted as a probability density function in Fig. 3a. A Gaussian fit (black line) to the histogram has a 1σ deviation of 0.16° which is less than the 1σ accuracy (yellow line in Fig. 3a) of the MMQ-G pitch measurement. This shows that the MMQ-G measures the aircraft pitch and roll angles with sufficient accuracy, which are then being used for real-time pointing corrections. Figure 3b shows the difference in desired elevation angle and the real-time elevation angle read back from the motor internal encoder as a probability density for the same flight. The 1σ of the Gaussian fit to the histogram (0.12°) is smaller than the resolution of the motor internal encoder confirming that the telescope position was corrected for the aircraft movements within our ability to read back the motor position.

A similar plot from a research flight (~ 4 h) on 16 July 2010 aboard the NOAA Twin Otter is shown in Fig. 3c and the 1σ of the Gaussian fit is 0.2° . This slightly larger distribution is within the resolution of the motor internal encoder. The fact that the 1σ for both platforms is less than or equal to the ability with which we can accurately

The CU Airborne MAX-DOAS instrument

S. Baidar et al.

Title Page

Abstract

Introduction

Conclusions

References

Tables

Figures



Back

Close

Full Screen / Esc

Printer-friendly Version

Interactive Discussion



read the position of the motor demonstrates that this motion compensation system is suitable for a wide range of moving platforms. Since the precision of the stepper motor is 0.01° , it is very likely that the difference between the real-time and desired elevation angle is smaller than what is being read back from the internal encoder and the overall angle accuracy (1σ) of the motion compensation system is better than 0.35° . The offset of 0.17° for the Gaussian fit in Fig. 3c is probably due to some remaining misalignment between the angle sensor and the motor but is smaller than the accuracy of the angle sensor.

The tolerance level (brown dashed lines in Fig. 3b, c) above which the motor performs an automatic reset was set to 0.7° (2σ theoretical accuracy) for the campaigns described here. The statistical distribution of the elevation angle difference indicates that the desired position of the motor was achieved after the reset.

2.6 Field deployment and operation during CalNex and CARES

The CU AMAX-DOAS instrument was deployed aboard the NOAA Twin Otter remote sensing research aircraft during the CalNex and CARES field campaigns from 19 May–19 July 2010 in California after test flights in 2008 and 2009. The pylon was modified significantly after 2009. The aircraft is an unpressurized twin engine turboprop with an altitude ceiling of ~ 4 km above sea level (without supplemental cabin oxygen). It has a normal cruising speed of $\sim 65 \text{ ms}^{-1}$ and ascent rate of $\sim 10 \text{ ms}^{-1}$ making it particularly suitable for surveying vertical and horizontal distributions of trace gases in a polluted urban environment. During CalNex, the NOAA Twin Otter aircraft was stationed at Ontario, CA, and joined the CARES campaign from 16–29 June 2010 at Sacramento, CA. The plane was equipped with a suite of remote sensing instruments: the University of Colorado deployed (1) CU AMAX-DOAS instrument, (2) two 4-channel radiometers (zenith and nadir viewing) to measure surface albedo; further, NOAA/ESRL/CSD deployed (3) a nadir-pointing Tunable Ozone Profiler for Aerosol and oZone (TOPAZ) lidar (Alvarez II et al., 2011), which measures vertical distribution of O_3 , and the (4) University of Leeds HALO Doppler lidar (Pearson et al., 2009), which

The CU Airborne MAX-DOAS instrument

S. Baidar et al.

Title Page

Abstract

Introduction

Conclusions

References

Tables

Figures



Back

Close

Full Screen / Esc

Printer-friendly Version

Interactive Discussion



measures 3-dimensional wind fields, as well as (5) a nadir pointing infrared pyrometer, and (6) an in-situ O₃ monitor.

The purpose of the CU AMAX-DOAS deployment was to measure horizontal and vertical distributions of NO₂, HCHO, CHOHO and aerosol extinction over California, particularly over the SCAB, characterize boundary conditions for comparison with atmospheric models, and probe for pollutant concentrations above the boundary layer. A total of 52 research flights, each lasting up to ~ 4 h, were carried out over the two months period (206 flight hours). Flight plans were developed with the scientific objectives of mapping out horizontal and vertical distribution as well as characterizing transport of pollutants and validation of satellite retrievals. As this was the first deployment of this specific instrument pylon, different integration times and EA sequences were explored as well as the LabVIEW acquisition software was updated during the early portion of the campaign for optimization. Spectra were collected with 2 s integration time during the second half of the campaign and all the data presented in this paper are 2 s data unless otherwise noted. The most commonly used EA sequence included EAs 90°(zenith), 20°, 10°, 5°, 2°, 0°, -2°, -5°, -10°, -20° and -90° (nadir) with 0° corresponding to a view parallel to the horizon. The FOV of the telescope at nadir viewing geometry gives a footprint of ~ 0.55 km while flying at 4 km altitude. Typically, nadir spectra were recorded every 12–15 s, corresponding to a horizontal resolution of ~ 1 km.

3 Data analysis

3.1 DOAS analysis

The measured spectra were analyzed for NO₂, CHOCHO, HCHO, H₂O and O₄ using the DOAS method (Platt and Stutz, 2008) implemented by the WinDOAS software (Fayt and Van Roozendael, 2001). In DOAS, measured spectra are analyzed against a Fraunhofer reference spectrum, and absorption cross-sections of different absorbers

The CU Airborne MAX-DOAS instrument

S. Baidar et al.

Title Page

Abstract

Introduction

Conclusions

References

Tables

Figures

◀

▶

◀

▶

Back

Close

Full Screen / Esc

Printer-friendly Version

Interactive Discussion



The CU Airborne MAX-DOAS instrument

S. Baidar et al.

Title Page

Abstract

Introduction

Conclusions

References

Tables

Figures

⏪

⏩

◀

▶

Back

Close

Full Screen / Esc

Printer-friendly Version

Interactive Discussion



in the atmosphere are fitted simultaneously in a selected wavelength interval applying a non-linear least-square fitting routine. A low order polynomial to account for scattering processes and broadband absorption in the atmosphere as well as broadband instrumental features, a Ring reference spectrum to account for the filling in of Fraunhofer lines due to rotational Raman scattering (Grainger and Ring, 1962), and an additional intensity offset to account for instrumental stray light were also included in the fitting procedure. The Ring spectrum is calculated from the Fraunhofer reference spectrum with the DOASIS software (Kraus, 2006). A high altitude (~ 4 km) zenith spectrum from a clean, cloud free region of the same flight was included for the analysis of the individual flight data. The choice of the zenith spectrum as Fraunhofer reference spectrum minimizes the amount of tropospheric absorbers in the reference spectrum, allowing for the detection of trace gases more sensitively. Since measured spectra are analyzed with respect to a reference spectrum, the quantity retrieved from the DOAS analysis is a differential slant column density (dSCD), which is the integrated excess concentration of the absorber along the light path length with respect to the reference. The trace gas absorption cross sections and analysis settings for the retrievals of the different trace gases are listed in Tables 1 and 2, respectively. Examples for spectral fits of NO_2 , CHOCHO, HCHO, O_4 , and H_2O from the data measured during CalNex and CARES campaigns are shown in Fig. 4. Detection limit for CU AMAX-DOAS instrument in clean FT and polluted urban BL such as the SCAB for 30 and 2 s integration time is listed in Table 3. It is roughly equivalent to the 3σ DOAS fit error for typical clean FT (near Rayleigh atmosphere) and polluted urban BL atmospheric conditions (see Fig. 10b for aerosol extinction profile). Note that detection limit highly depends upon the atmospheric conditions during the time of measurement. The quantity retrieved from a DOAS analysis, the dSCD is converted to VCD by using an air mass factor (AMF). The VCD is the integral absorber concentration per unit area.

$$\text{VCD} = \frac{\text{dSCD}}{\text{dAMF}} \quad (1)$$

**The CU Airborne
MAX-DOAS
instrument**

S. Baidar et al.

dAMF is usually calculated with the help of a radiative transfer program to convert the measured dSCD to a VCD. It requires a-priori knowledge of trace gas vertical concentrations and aerosol extinction coefficients along with other input parameters such as pressure, temperature, surface albedo (SA), aerosol asymmetry parameter, g , and aerosol single scattering albedo (SSA). NO_2 concentrations, profile shapes and aerosol scenarios are highly variable in the SCAB because of the variable sources and hence the probability of introducing a significant amount of error in radiative transfer calculations of AMFs is very high. Instead, we applied a simple geometric approximation for the nadir viewing geometry to convert dSCDs to VCDs. The geometric approach, its validity and error associated with this approximation are further discussed in Sect. 3.3.

3.2 Radiative transfer modeling

Since the AMAX-DOAS measurements are carried out in the open atmosphere using scattered sun light as the light source, the solar radiative transfer during the time of measurement needs to be modeled to interpret the retrieved data. The radiative transfer program McArtim (Monte Carlo atmospheric radiative transfer inversion model) (Deutschmann et al., 2011) used here is a fully spherical model and simulates radiative transfer in the atmosphere in the UV/vis/NIR spectral range using a Monte Carlo approach. In McArtim, the 3-D atmosphere is simulated as a 1-D modeled atmosphere divided in concentric spherical shells. The atmospheric conditions during the time of measurement in each vertical layer are assumed to be horizontally and vertically homogeneous. McArtim has the capability to simulate SCDs and AMFs of trace gases and aerosols needed for the interpretation of AMAX-DOAS data. Auxiliary input parameters used in the radiative transfer program were either measured aboard the aircraft (i.e. surface albedo), on the ground at CalNex ground site (Ryerson et al., 2012) (i.e. aerosol single scattering albedo), California Air Resources Board (CARB) (<http://www.arb.ca.gov/homepage.htm>) monitoring stations or typical values for urban environments based on previous studies (e.g. Dubovik et al., 2002).

[Title Page](#)[Abstract](#)[Introduction](#)[Conclusions](#)[References](#)[Tables](#)[Figures](#)[Back](#)[Close](#)[Full Screen / Esc](#)[Printer-friendly Version](#)[Interactive Discussion](#)

3.3 Geometric approximation for conversion of dSCDs to VCDs

Under the geometric approximation, it is assumed that all the photons get scattered only once very close to the ground or are reflected from the surface before entering the telescope in nadir geometry. The geometric air mass factor (geoAMF) is then only a function of the solar zenith angle (SZA) and is given by

$$\text{geoAMF} = 1 + \frac{1}{\cos(\text{SZA})} \quad (2)$$

The schematic of the geometric approximation is shown in the Fig. 1 inset.

In our DOAS analysis, a high altitude zenith spectrum from a clean background area is used as reference spectrum. Assuming this background zenith spectrum has no tropospheric NO₂, the nadir dSCDs can be considered as tropospheric SCDs for most flight performed at low SZA. At high SZA, stratospheric NO₂ contribution changes with SZA and hence requires independent removal. For such flights (18 out of 52), stratospheric NO₂ contribution was corrected by fitting a polynomial through all the zenith dSCDs above 1.8 km flight altitude and subtracting the polynomial from the nadir measurements. The resulting quantity is defined as the tropospheric SCDs. This quantity is then converted to VCD ($\text{VCD} = \text{SCD}/\text{geoAMF}$), and is defined as VCD below the aircraft.

Sensitivity studies using the radiative transfer model (RTM), McArtim were performed to estimate uncertainties associated with the geometric approximation. A range of conditions that could potentially occur during the time of measurements were explored for this study. A representative sample of the results is summarized in Table 4, as the relative error in the geoAMF assumption compared to AMFs calculated using the RTM for different scenarios specified in the table. The results for the most likely atmospheric state in the SCAB (surface albedo, SA = 0.1; single scattering albedo, SSA = 0.94; asymmetry parameter, $g = 0.68$; AOD = 0.4, boundary layer height BLH = 1.0 km; NO₂ = 10 ppb) is also shown in Table 4; it is based on ancillary measurements aboard the aircraft, CalNex ground site at Pasadena, CA and CARB

Title Page

Abstract

Introduction

Conclusions

References

Tables

Figures

◀

▶

◀

▶

Back

Close

Full Screen / Esc

Printer-friendly Version

Interactive Discussion



**The CU Airborne
MAX-DOAS
instrument**S. Baidar et al.

[Title Page](#)[Abstract](#)[Introduction](#)[Conclusions](#)[References](#)[Tables](#)[Figures](#)[⏪](#)[⏩](#)[◀](#)[▶](#)[Back](#)[Close](#)[Full Screen / Esc](#)[Printer-friendly Version](#)[Interactive Discussion](#)

ground monitoring stations. Thomson et al. (2012) reported an average value for SSA of 0.92 at 532 nm during the entire CalNex campaign at Pasadena. They find SSA values to be slightly higher during the day time, when our measurements were taken. AOD measured at the AERONET station at Pasadena, CA showed AOD values to be lower than 0.4 at 440 nm for almost all of summer 2010, and the AOD of 0.4 likely represents an upper limit to provide a conservative estimate of relative error. It should be noted that these quantities are wavelength dependent. The largest source of error was found to be surface albedo (see Table 4), which is constrained using the measurement aboard the aircraft. Notably, our SA measurements also provide means to filter data for conditions where the error may exceed 10%. The error from using the geoAMF compared to AMF calculated for the most likely atmospheric state in SCAB is plotted as a function of SZA in Fig. 5. Based on this, a SZA cutoff of 65° was used to constrain the error in the NO₂ vertical columns (85% of flight time with SZA < 65°). With these filters, the error in geoAMF is < 7% for most conditions, and slightly larger (error < 25% in all cases) for SZA ~ 65° or during high altitude flights over low surface albedo. The error associated with the geoAMF is consistent with previous airborne DOAS studies which used the geometric approximation. Melamed et al. (2003) estimated the error in NO₂ VCD from the geometric approximation to be ~ 20% based on the discrepancies between measured and modeled O₂ AMF. To the best of our knowledge, there have been no previous deployments of AMAX-DOAS with simultaneous SA measurements by independent sensors. The higher SA (~ 10% at 479 nm) is found widespread in the SCAB, and has the favorable effect to reduce errors from the geoAMF assumption due to compensating effects in the radiative transfer calculations.

3.4 Aerosol extinction profile retrieval

In the near-UV and visible wavelength range, the change in photon path length compared to a Rayleigh atmosphere and hence the measured dSCDs of a trace gas depends mainly on the aerosol extinction profile. Thus, if the vertical distribution of an absorber is well known, the dSCD measurements of such species can be exploited to infer

The CU Airborne MAX-DOAS instrument

S. Baidar et al.

Title Page

Abstract

Introduction

Conclusions

References

Tables

Figures

⏪

⏩

◀

▶

Back

Close

Full Screen / Esc

Printer-friendly Version

Interactive Discussion



aerosol properties. The collisional complex of oxygen, O_4 is one such species (Honninger et al., 2004; Wagner et al., 2004; Wittrock et al., 2004; Clemer et al., 2010). The O_4 concentration varies with pressure, temperature and square of the concentration of O_2 . Hence, the dSCD measurements of O_4 can be used to calculate aerosol extinction profiles. O_4 dSCD measurements from ground-based and airborne MAX-DOAS have previously been used for aerosol extinction profile and aerosol optical depth (AOD) retrievals (Clemer et al., 2010; Merlaud et al., 2011 and references within). We used an iterative forward model approach to obtain the aerosol extinction profile. Under this approach a set of measured O_4 SCDs, \mathbf{y} , is related to the aerosol extinction vertical profile, \mathbf{x} , by forward model F such that

$$\mathbf{y} = F(\mathbf{x}, \mathbf{b}) + \varepsilon \quad (3)$$

where \mathbf{b} are forward model parameters that are not retrieved and ε is the sum of measurement and model errors. For 0° EA, i.e. parallel to the horizon, the measurement is almost entirely sensitive to the altitude of measurement and almost all of the information contained in the SCD comes from that particular altitude. We exploit this property and retrieve the aerosol extinction profile by using a modified onion peeling algorithm using 0° EA O_4 SCD measurements. First the extinction above the highest altitude is constrained using upward EA scans performed at that altitude. Then the aerosol extinction values at the subsequent altitudes during the descent are determined using the set of 0° EA O_4 SCD measurements at those altitudes. Aerosol extinction below the lowest aircraft altitude is obtained using downward EA scans performed at the lowest altitude. The process is iterated to account for any information on O_4 SCDs for 0° EA at a given altitude from O_4 column below the measurement altitude, until measured and modeled O_4 SCDs agree. The profile is then verified using other angles in the EA scans during the descent/ascent. It should be noted that this approach is feasible only due to the ability to maintain the desired EAs within narrow error bound also during descent/ascent of the aircraft, as discussed in Sect. 2.5.

**The CU Airborne
MAX-DOAS
instrument**

S. Baidar et al.

Title Page

Abstract

Introduction

Conclusions

References

Tables

Figures

◀

▶

◀

▶

Back

Close

Full Screen / Esc

Printer-friendly Version

Interactive Discussion



The relative error in O_4 SCDs at different altitudes in the atmosphere for different pointing uncertainties for a 0° EA is illustrated in Fig. 6. An uncertainty of $1\text{--}2^\circ$, which can easily happen on an airborne platform, could result in 20–80 % error above 10 km. Considering a non-linear relationship between O_4 SCD and aerosol extinction, this could result in even larger errors when O_4 SCDs are used to retrieve the aerosol extinction profile. This highlights the need for a motion compensation system to maintain pointing accuracy of the telescope.

Sensitivity studies were performed to estimate the error in the retrieved aerosol extinction profile due to uncertainties in model parameters and angle accuracy. We studied the effects of SA, SSA, asymmetry parameter, temperature, and angle uncertainty of the telescope on aerosol extinction coefficients at 477 nm. Results from the study are summarized in Table 5. The asymmetry parameter uncertainty ($g = 0.68$ to 0.75) could result in as much as 10 % relative error in extinction values. A 5°C temperature uncertainty could also result in similar relative error as the O_4 concentration in the atmosphere is temperature dependent (density effect). We used temperature measured aboard the aircraft to minimize this error. Angle accuracy uncertainty was found to result in large extinction errors ($> 0.01 \text{ km}^{-1}$) in the transition layer at the top of the boundary layer and around elevated layers. It points to the possibility of uncertainty in altitude of aerosol layers in the extinction profile. Angle accuracy uncertainties to our knowledge have not previously been considered for error estimates for vertical profiles from airborne DOAS measurements, but it could be the most important and largest source of error in the retrieved profiles, especially for transition layers.

3.5 Trace gas vertical profile retrieval

Trace gas vertical profile retrieval algorithm is based on the concept of Optimal Estimation (Rodgers, 2000). The use of this technique for profile retrieval from AMAX-DOAS measurements have been described in detail before (e.g. Bruns et al., 2004) and hence will only be introduced here briefly. A set of measurements y , which in our case are

trace gas SCDs for different LOS can be related to a vertical distribution, x by the forward model F as shown in Eq. (3).

Equation (3) can be rewritten in a linearized form as:

$$\mathbf{y} = \mathbf{K}\mathbf{x} + \varepsilon \quad (4)$$

where \mathbf{K} defined as $\frac{\partial \text{SCD}_i}{\partial x_j}$ is the weighting function matrix which expresses the sensitivity of a measurement, \mathbf{y} to \mathbf{x} . We used the maximum a posterior solution as described in Rodgers (2000) to solve Eq. (4):

$$\mathbf{x} = \mathbf{x}_a + \left(\mathbf{K}^T \mathbf{S}_\varepsilon^{-1} \mathbf{K} + \mathbf{S}_a \right)^{-1} \mathbf{K}^T \mathbf{S}_\varepsilon^{-1} (\mathbf{y} - \mathbf{K}\mathbf{x}_a) \quad (5)$$

where \mathbf{x}_a is the a priori profile and \mathbf{S}_a and \mathbf{S}_ε are the a priori error and measurement error covariance matrices, respectively. The a priori profile is used to constrain the above described problem as it is generally ill-posed.

The solution given by Eq. (5) is a weighted mean of the a priori profile and the information from the measurement. This weight is given by the averaging kernel matrix \mathbf{A} ,

$$\mathbf{A} = \left(\mathbf{K}^T \mathbf{S}_\varepsilon^{-1} \mathbf{K} + \mathbf{S}_a \right)^{-1} \mathbf{K}^T \mathbf{S}_\varepsilon^{-1} \mathbf{K} \quad (6)$$

The retrieval at any layer is an average of the whole profile weighted by the row of the averaging kernel matrix corresponding to that layer. The averaging kernel matrix also contains information about the number of independent pieces of information retrieved, and an estimate of the vertical resolution of the retrieved profile at a given level. The trace of the averaging kernel matrix, \mathbf{A} , gives the degrees of freedom (DOF), i.e. number of independent pieces of information retrieved. The FWHM of the main peak of an averaging kernel at any layer gives the estimate of the vertical resolution of the retrieved profile at that layer. For an ideal retrieval scenario, \mathbf{A} is the identity matrix, the DOF equal the number of retrieved profile layers and the averaging kernels peak at their corresponding altitudes. In reality, the retrieved profile is a smoothed version of the true profile.

The CU Airborne
MAX-DOAS
instrument

S. Baidar et al.

Title Page

Abstract

Introduction

Conclusions

References

Tables

Figures

◀

▶

◀

▶

Back

Close

Full Screen / Esc

Printer-friendly Version

Interactive Discussion



4 Results and discussion

4.1 Horizontal distribution of NO₂

As an example, a map of NO₂ VCD distribution in the SCAB from RF# 46 on 16 July 2010 (10:30–14:10 PDT) is shown in Fig. 7. The small footprint (~ 1 km along the flight track) of the measurement allows us to clearly identify local hotspots and pollution sources. The NO₂ map in Fig. 7 reflects our understanding of the NO_x sources and its relatively short life time (~ 4 h). Clear NO₂ hotspots can be observed around downtown Los Angeles and Ontario, along the major highway, State Route 210 and at intersections of major highways. In contrast, very little NO₂ is seen in the eastern part of the basin, and over the High Desert to the northeast, where there are no significant local sources of NO_x. The footprint of CU AMAX-DOAS is comparable to air quality models, and smaller than that of current solar stray light satellite observations, which also measure VCDs of trace gases; this makes this data set an excellent opportunity to evaluate emissions in air quality models and validate satellite observations. A first application of CU AMAX-DOAS to test NASA NO₂ VCD retrievals from the OMI/AURA satellite instrument is currently in preparation (Oetjen et al., 2012).

4.2 Validation of NO₂ vertical column

To validate the retrieval of our NO₂ VCDs by CU AMAX-DOAS using the geometric approximation, we compare our observations with NO₂ VCDs from ground based MAX-DOAS instruments. Two CU GMAX-DOAS instruments (Sinreich et al., 2010; Coburn et al., 2011) were deployed at the CalNex ground site (Ryerson et al., 2012) in Pasadena, CA, the Fontana Arrows CARB monitoring network station and the CARES T1 (Zaveri et al., 2012) site in Cool, CA at various times of the campaign. GMAX-DOAS operates in the same principle as AMAX-DOAS. Spectra measured at off-axis angles were analyzed for NO₂ using a closest zenith reference spectrum in time. The retrieved NO₂ dSCDs for 20° EA were converted to VCDs using a dAMF calculated by McArtim.

AMTD

5, 7243–7292, 2012

The CU Airborne MAX-DOAS instrument

S. Baidar et al.

Title Page

Abstract

Introduction

Conclusions

References

Tables

Figures

◀

▶

◀

▶

Back

Close

Full Screen / Esc

Printer-friendly Version

Interactive Discussion



4.3 Determination of O₄ SCD in the reference spectrum

The scale height of O₄ in the atmosphere is ~ 4 km and as our measurements were usually performed below 4 km altitude, it is important to quantify the O₄ SCD contained in the reference spectrum (SCD_{ref}) in order to accurately retrieve the aerosol extinction profile. Merlaud et al. (2011) used a linear regression between measured dSCD and calculated SCD using RTM for airborne measurements above 5.5 km in the Arctic to determine SCD_{ref} and the dSCD correction factor, α :

$$\text{SCD} = \alpha \times \text{dSCD} + \text{SCD}_{\text{ref}} \quad (7)$$

A dSCD correction factor (α) for O₄ dSCD measurements has been used to retrieve aerosol extinction from MAX-DOAS measurements. The value for the correction factor is different between different environments and research groups, and wavelength, and ranges from 0.75 to 0.89 (Wagner et al., 2009; Clemer et al., 2010; Merlaud et al., 2011; Zieger et al., 2011). The source for a need of α is currently not well understood. It has been speculated that the need for α could be due to the temperature dependence of the O₄ absorption cross-section (Wagner et al., 2009; Clemer et al., 2010). Indeed, a temperature uncertainty in the O₄ absorption cross-section has been reported (Wagner et al., 2002).

We employed the same approach as Merlaud et al. (2011) to determine SCD_{ref} and α . Temperature and pressure as measured on the plane were used to prescribe the vertical distribution of O₄ in the model. Temperature and pressure profiles were extrapolated to the ground using the lapse rate and scale height determined from the measurements, respectively. The temperature at the ground was 36.7 °C and the pressure was 966 mbar at the ground. Comparison of extrapolated temperature and pressure values at the ground with measurements at the nearest CARB monitoring stations showed good agreement within ± 2 °C and ± 10 mbar, respectively. Profiles above the aircraft were extrapolated based on the mean temperature and pressure profiles measured at Joshua Tree, CA. The O₃ profile was also constructed similarly and was measured by the NOAA TOPAZ lidar aboard the plane. Based on the regression analysis,

Title Page

Abstract

Introduction

Conclusions

References

Tables

Figures

◀

▶

◀

▶

Back

Close

Full Screen / Esc

Printer-friendly Version

Interactive Discussion



$\alpha = 0.99 \pm 0.01$ for 477 nm and hence it was concluded that a scaling factor was not needed to explain our measurements. Figure 9 shows a correlation analysis between simulated O₄ SCDs with our retrieved aerosol profile (see Fig. 10a) and measured O₄ SCDs at 477 nm for a low approach at Brackett airfield during RF#46 (see more details below). Low approach is a maneuver over an airport in which the pilot intentionally does not make a contact with the runway. An O₄ reference SCD of 9×10^{42} molecule² cm⁻⁵ based on the regression has been added to the measured dSCDs to convert them to SCDs.

4.4 Examples of retrieved vertical profiles

Figures 10 and 11 show retrieved vertical profiles of aerosol extinction coefficient and trace gas mixing ratio for the above mentioned low approach during RF#46. The aircraft was flying at ~ 3.1 km above ground level (AGL), made a slow descent to an altitude of ~ 0.6 km AGL at the airport, and then ascended again. The telescope was scanning a set of EAs (-90° , -5° , -2° , 0° , 2° , 5° , 90°) during the low approach. A complete set of EAs was also measured at the highest altitude just before the descent and at the lowest point before starting to ascent in order to characterize the air mass above and below the aircraft. The descent portion of the low approach took ~ 8 min.

4.4.1 Aerosol extinction coefficient profiles

Aerosol extinction coefficient vertical distribution retrieved at 477 nm is shown in Fig. 10b. The extinction profile was retrieved by iteratively minimizing the residual between measured and simulated O₄ SCDs, see Sect. 3.4. Figure 10a illustrates the agreement between the measured and modeled O₄ SCDs at 477 nm for EA 0° . The corresponding aerosol extinction profile is presented in Fig. 10b. The aerosol extinction profile in Fig. 10b indicates that most of the aerosols are located inside the boundary layer (up to 0.9 km, indicated by the decrease in NO₂ and aerosol) with a 500 m thick elevated layer at ~ 2.5 km. Error contribution in retrieved extinction due EA uncertainty

Title Page

Abstract

Introduction

Conclusions

References

Tables

Figures

◀

▶

◀

▶

Back

Close

Full Screen / Esc

Printer-friendly Version

Interactive Discussion



of 0.35° is shown Fig. 10c and illustrates that pointing accuracy is needed especially to minimize error in transition layers and elevated layers.

Integration of the extinction coefficient profile over altitude gives AOD, the total load of aerosols in the atmosphere. AOD at 477 nm from the profile in Fig. 10b is 0.16 ± 0.03 , and agrees well with 0.18 ± 0.02 at 500 nm measured by AERONET station located at Pasadena. The AOD values for the Aeronet station reported here are hourly averages and standard deviations for the hour of the low approach. Pasadena is located 30 km west of the Brackett airfield; the telescope was pointing towards the west during our low approach, and measurements inherently average over spatial scales of typically few 10 km. The excellent agreement between the AOD calculated from our profiles and AERONET station adds confidence to our retrieval approach and accuracy of the retrieved profile. To our knowledge this is the first demonstration of quantitative retrieval of aerosol extinction from O_4 dSCD observations that does not require a correction factor.

4.4.2 Trace gas vertical profiles

Figure 11 shows the retrieved NO_2 , CHOCHO, HCHO and H_2O mixing ratio profiles from the same low approach. NO_2 , CHOCHO, and HCHO vertical profiles have a very similar shape, with most of the trace gases located inside the boundary layer. This is not surprising since most of the sources for these gases are close to the surface. On the other hand, the H_2O profile is almost linearly decreasing with altitude. The retrieved NO_2 profile shows an average urban boundary layer value of 14.2 ± 1.5 ppb (at the surface: $1 \text{ ppb} \cong 2.46 \times 10^{10}$ molecules cm^{-2} at sea level, and 298 K temperature). The hourly NO_2 data recorded at the nearest CARB monitoring station at Pomona is 13 ppb. Pomona station is located ~ 3 km south of the Brackett airfield. Our retrieved NO_2 surface mixing ratio agrees well with the measurement at the ground station. The CHOCHO profile shows a BL value of 274 ± 48 ppt. It also exhibits an elevated layer of glyoxal with $\sim 33 \pm 8$ ppt at around 2.5 km (Fig. 11b). The lower error bars in the free troposphere compared to the BL is due to two reasons: (1) the dSCD retrieval

The CU Airborne MAX-DOAS instrument

S. Baidar et al.

Title Page

Abstract

Introduction

Conclusions

References

Tables

Figures

◀

▶

◀

▶

Back

Close

Full Screen / Esc

Printer-friendly Version

Interactive Discussion



**The CU Airborne
MAX-DOAS
instrument**

S. Baidar et al.

the retrieved profile to different a priori profiles was also tested, and resulted in small changes, inside the BL, which were always within the error bars shown. The lower averaging kernels below 600 m are explained from the observing geometry of the low approach (see above). While this decrease in sensitivity for other EAs compared to 0° for a given atmospheric layer does not appear to limit our ability to infer meaningful information near the surface (see this section above), it highlights the benefit of capabilities to maintain EA = 0° during aircraft ascent/descent to systematically probe the atmosphere with maximum sensitivity, and vertical resolution.

5 Conclusions

An Airborne MAX-DOAS instrument equipped with a motion-stabilized scanning telescope to collect solar stray light photons provides accurate means to probe atmospheric composition in terms of the horizontal and vertical distributions of multiple trace gases and aerosols simultaneously and sensitively by means of a single, portable, instrument.

The CU AMAX-DOAS instrument is validated by comparison with NO_2 VCDs measured by ground-based MAX-DOAS. A sensitivity study using radiative transfer modeling reveals that the geometric approximation is a viable option to convert NO_2 dSCD to VCD for measurements below the plane. This approximation is found to be accurate over Southern California, where elevated surface albedo ($\sim 10\%$ at 479 nm, measured aboard the plane) compensates for reduced sensitivity due to aerosols. We estimate the error in the NO_2 vertical columns due to the geometric approximation to be less than 7% under most conditions for $\text{SZA} < 65^\circ$; a slightly larger error ($< 25\%$ in all cases) is found for $\text{SZA} \sim 65^\circ$ or during high altitude flights over low surface albedo. These results emphasize benefits of measuring surface albedo and AOD by independent sensors.

For a case study, vertical profiles of NO_2 , CHOCHO, HCHO, H_2O , and aerosol extinction coefficient at 477 nm showed that trace gases and aerosols are located mostly

[Title Page](#)[Abstract](#)[Introduction](#)[Conclusions](#)[References](#)[Tables](#)[Figures](#)[⏪](#)[⏩](#)[◀](#)[▶](#)[Back](#)[Close](#)[Full Screen / Esc](#)[Printer-friendly Version](#)[Interactive Discussion](#)

inside the BL, though the presence of elevated layer was observed as well. Sensitivity studies show that the main error source in the retrieved vertical profiles of aerosol extinction coefficient is the uncertainty in the asymmetry parameter of aerosol scattering. Further, sensitivity studies highlight the need of pointing accuracy of the telescope on moving platforms like an aircraft to accurately retrieve vertical distributions of trace gases and aerosol extinction coefficients. The accuracy of our motion compensation system is found to be $< 0.35^\circ$ by comparison with an independent inertial system.

An ~ 500 m thick layer at around 2.5 km altitude AGL was observed that was decoupled from the BL, and contained 33 ± 8 ppt CHOCHO, NO_2 below the detection limit (30 ppt, for 2 s integration time), 545 ± 114 ppt HCHO, $0.029 \pm 0.004 \text{ km}^{-1} \epsilon_{477}$, corresponding to a partial vertical columns of $4.14 \pm 1.12 \times 10^{13}$ molecules cm^{-2} CHOCHO, $7.10 \pm 1.75 \times 10^{14}$ molecules cm^{-2} HCHO, and partial AOD of 0.047 ± 0.007 at 477 nm. This elevated layer contained ratios of CHOCHO/HCHO of 0.06 ± 0.02 , compared to 0.027 ± 0.006 inside the BL. The concurrent location of elevated aerosol extinction at the same altitude indicates either collocated glyoxal sources from VOC oxidation, or the release of glyoxal that was initially taken up as SOA back to the gas-phase. The increase in the CHOCHO/HCHO ratio with altitude appears to be outside error bars, and the cause for this altitude dependence deserves further investigation.

The capabilities of CU AMAX-DOAS are not limited to the parameters presented here, and also include measurements of reactive species, like halogen oxide radicals, and aerosols extinction coefficients at other wavelengths. The absence of sampling lines, and inherent averaging over extended spatial scales enable the AMAX-DOAS technique to bridge between ground-based networks, atmospheric models, and satellites, and holds as yet unexplored potential to advance airborne atmospheric observations, and improve our understanding of the processes taking place in the atmosphere. The CU AMAX-DOAS deployment during the CalNex and CARES field campaigns makes a 10 week long data set available that we plan to apply for such studies.

**The CU Airborne
MAX-DOAS
instrument**

S. Baidar et al.

Title Page

Abstract

Introduction

Conclusions

References

Tables

Figures

◀

▶

◀

▶

Back

Close

Full Screen / Esc

Printer-friendly Version

Interactive Discussion



Appendix A

List of frequently used abbreviations

AGL	above ground level
AMAX-DOAS	airborne multi-axis differential optical absorption spectroscopy
AMF	air mass factor
AOD	aerosol optical depth
BL	boundary layer
BLH	boundary layer height
CalNex	California Research at the Nexus of Air Quality and Climate Change
CARB	California Air Resources Board
CARES	Carbonaceous Aerosols and Radiative Effects Study
dAMF	differential air mass factor
dSCD	differential slant column density
DOF	degrees of freedom
EA	elevation angle
FOV	field of view
FT	free troposphere
FWHM	full width at half maximum
geoAMF	geometric air mass factor
LOS	lines of sight
MAX-DOAS	multi-axis differential optical absorption spectroscopy
RF	research flight
RTM	radiative transfer model
SA	surface albedo
SCD	slant column density
SCAB	South Coast Air Basin

The CU Airborne MAX-DOAS instrument

S. Baidar et al.

Title Page

Abstract

Introduction

Conclusions

References

Tables

Figures

◀

▶

◀

▶

Back

Close

Full Screen / Esc

Printer-friendly Version

Interactive Discussion



SOA secondary organic aerosol
SSA single scattering albedo
SZA solar zenith angle
VCD vertical column density

Acknowledgements. This work was supported by the California Air Resource Board (CARB) contract 09-317, the National Science Foundation CAREER award ATM-847793, CU startup-funds (RV) and an ESRL-CIRES Graduate Fellowship (SB). The authors like to thank Tim
5 Deutschmann, University of Heidelberg for the radiative transfer code, McArtim, David Thomson for the software support, Caroline Fayt and Michel van Roozendael for the WINDOAS software and the NOAA Twin Otter research flight crew.

References

- 10 Alvarez II, R. J., Senff, C. J., Langford, A. O., Weickmann, A. M., Law, D. C., Machol, J. L., Merritt, D. A., Marchbanks, R. D., Sandberg, S. P., Brewer, W. A., Hardesty, R. M., and Banta, R. M.: Development and application of a compact, tunable, solid-state airborne ozone lidar system for boundary layer profiling, *J. Atmos. Ocean. Tech.*, 28, 1258–1272, doi:10.1175/JTECH-D-10-05044.1, 2011.
- 15 Bogumil, K., Orphal, J., Homann, T., Voigt, S., Spietz, P., Fleischmann, O., Vogel, A., Hartmann, M., Kromminga, H., Bovensmann, H., Frerick, J., and Burrows, J.: Measurements of molecular absorption spectra with the SCIAMACHY pre-flight model: instrument characterization and reference data for atmospheric remote-sensing in the 230–2380 nm region, *J. Photochem. Photobiol. A.*, 157, 167–184, doi:10.1016/S1010-6030(03)00062-5, 2003.
- 20 Bruns, M., Buehler, S. A., Burrows, J. P., Heue, K. P., Platt, U., Pundt, I., Richter, A., Rozanov, A., Wagner, T., and Wang, P.: Retrieval of profile information from airborne multi axis UV/visible skylight absorption measurements, *Appl. Optics*, 43, 4415–4426, doi:10.1364/AO.43.004415, 2004.
- 25 Bruns, M., Buehler, S. A., Burrows, J. P., Richter, A., Rozanov, A., Wang, P., Heue, K. P., Platt, U., Pundt, I., and Wagner, T.: NO₂ Profile retrieval using airborne multi axis UV-visible skylight absorption measurements over central Europe, *Atmos. Chem. Phys.*, 6, 3049–3058, doi:10.5194/acp-6-3049-2006, 2006.

The CU Airborne MAX-DOAS instrument

S. Baidar et al.

Title Page

Abstract

Introduction

Conclusions

References

Tables

Figures

◀

▶

◀

▶

Back

Close

Full Screen / Esc

Printer-friendly Version

Interactive Discussion



**The CU Airborne
MAX-DOAS
instrument**S. Baidar et al.

Title Page

Abstract

Introduction

Conclusions

References

Tables

Figures

◀

▶

◀

▶

Back

Close

Full Screen / Esc

Printer-friendly Version

Interactive Discussion



Clémer, K., Van Roozendael, M., Fayt, C., Hendrick, F., Hermans, C., Pinardi, G., Spurr, R., Wang, P., and De Mazière, M.: Multiple wavelength retrieval of tropospheric aerosol optical properties from MAXDOAS measurements in Beijing, *Atmos. Meas. Tech.*, 3, 863–878, doi:10.5194/amt-3-863-2010, 2010.

5 Coburn, S., Dix, B., Sinreich, R., and Volkamer, R.: The CU ground MAX-DOAS instrument: characterization of RMS noise limitations and first measurements near Pensacola, FL of BrO, IO, and CHOCHO, *Atmos. Meas. Tech.*, 4, 2421–2439, doi:10.5194/amt-4-2421-2011, 2011.

Deutschmann, T., Beirle, S., Friess, U., Grzegorski, M., Kern, C., Kritten, L., Platt, U., Prados-Roman, C., Pukite, J., Wagner, T., Werner, B., and Pfeilsticker, K.: The Monte Carlo atmospheric radiative transfer model McArtim: introduction and validation of Jacobians and 3D features, *J. Quant. Spectrosc. Ra.*, 112, 1119–1137, doi:10.1016/j.jqsrt.2010.12.009, 2011.

10 Dix, B., Brenninkmeijer, C. A. M., Frieß, U., Wagner, T., and Platt, U.: Airborne multi-axis DOAS measurements of atmospheric trace gases on CARIBIC long-distance flights, *Atmos. Meas. Tech.*, 2, 639–652, doi:10.5194/amt-2-639-2009, 2009.

Dubovik, O., Holben, B., Eck, T. F., Smirnov, A., Kaufman, Y. F., King, M. D., Tanrè, D., and Slutsker, I.: Variability of absorption and optical properties of key aerosol types observed in worldwide locations, *J. Atmos. Sci.*, 59, 590–608, doi:10.1175/1520-0469(2002)059<0590:VOAAOP>2.0.CO;2, 2002.

20 Fayt, C. and Van Roozendael, M.: WinDOAS 2.1, Software User Manual, Belgian Institute for Space Aeronomy, Brussels, Belgium, available at: <http://uv-vis.aeronomie.be/software/WinDOAS/WinDOAS-SUM-210b.pdf> (last access: 29 May 2012), 2001.

Grainger, J. and Ring, J.: Anomalous Fraunhofer line profiles, *Nature*, 193, 762, doi:10.1038/193762a0, 1962.

25 Greenblatt, G. D., Orlando, J. J., Burkholder, J. B., and Ravishankara, A. R.: Absorption measurements of oxygen between 330 nm and 1140 nm, *J. Geophys. Res.*, 95, 18577–18582, doi:10.1029/JD095iD11p18577, 1990.

Hermans, C.: Measurement of absorption cross sections and spectroscopic molecular parameters: O₂ and its collisional induced absorption, available at: <http://spectrolab.aeronomie.be/o2.htm> (last access: 29 May 2012), 2002.

30 Heue, K.-P., Richter, A., Bruns, M., Burrows, J. P., v. Friedeburg, C., Platt, U., Pundt, I., Wang, P., and Wagner, T.: Validation of SCIAMACHY tropospheric NO₂-columns with AMAXDOAS measurements, *Atmos. Chem. Phys.*, 5, 1039–1051, doi:10.5194/acp-5-1039-2005, 2005.

**The CU Airborne
MAX-DOAS
instrument**

S. Baidar et al.

Title Page

Abstract

Introduction

Conclusions

References

Tables

Figures

◀

▶

◀

▶

Back

Close

Full Screen / Esc

Printer-friendly Version

Interactive Discussion



Hönninger, G., von Friedeburg, C., and Platt, U.: Multi axis differential optical absorption spectroscopy (MAX-DOAS), *Atmos. Chem. Phys.*, 4, 231–254, doi:10.5194/acp-4-231-2004, 2004.

Kraus, S.: A Framework Design for DOAS, Ph.D. thesis/masters, University of Heidelberg, Germany, 2006.

Liggio, J., Li, S., and McLaren, R.: Reactive uptake of glyoxal by particulate matter, *J. Geophys. Res.*, 110, D10304, doi:10.1029/2004JD005113, 2005.

Melamed, M. L., Solomon, S., Daniel, J. S., Langford, A. O., Portmann, R. W., Ryerson, T. B., Nicks, D. K. J., and McKeen, S. A.: Measuring reactive nitrogen emissions from point sources using visible spectroscopy from aircraft, *J. Environ. Monit.*, 5, 29–34, doi:10.1039/B204220G, 2003.

Melamed, M. L., Langford, A. O., Daniel, J. S., Portmann, R. W., Miller, H. L., Eubank, C. S., Schofield, R., Holloway, J., and Solomon, S.: Sulfur dioxide emission flux measurements from point sources using airborne near ultraviolet spectroscopy during the New England Air Quality Study 2004, *J. Geophys. Res.*, 113, D02305, doi:10.1029/2007JD008923, 2008.

Meller, R. and Moortgat, G.: Temperature dependence of the absorption cross sections of formaldehyde between 223 and 323 K in the wavelength range 225–375 nm, *J. Geophys. Res.*, 105, 7089–7101, doi:10.1029/1999JD901074, 2000.

Merlaud, A., Van Roozendaal, M., Theys, N., Fayt, C., Hermans, C., Quennehen, B., Schwarzenboeck, A., Ancellet, G., Pommier, M., Pelon, J., Burkhardt, J., Stohl, A., and De Mazière, M.: Airborne DOAS measurements in Arctic: vertical distributions of aerosol extinction coefficient and NO₂ concentration, *Atmos. Chem. Phys.*, 11, 9219–9236, doi:10.5194/acp-11-9219-2011, 2011.

Oetjen, H., Baidar, S., Krotkov, N. A., Lamsal, L. N., and Volkamer, R.: Airborne MAX-DOAS measurements over California: testing the NASA OMI tropospheric NO₂ product, *J. Geophys. Res.*, in preparation, 2012.

Ortega, I., Baidar, S., Coburn, S., Dix, B., Oetjen, H., Sinreich, R., and Volkamer, R.: Comparison of regularization and optimal estimation inversion techniques to retrieve trace gas profiles from ground-based MAX-DOAS, *Atmos. Meas. Tech. Discuss.*, in preparation, 2012.

Pearson, G., Davies, F., and Collier, C.: An analysis of the performance of the UFAM pulsed doppler lidar for observing the boundary layer, *J. Atmos. Ocean. Tech.*, 26, 240–250, doi:10.1175/2008JTECHA1128.1, 2009.

**The CU Airborne
MAX-DOAS
instrument**

S. Baidar et al.

[Title Page](#)[Abstract](#)[Introduction](#)[Conclusions](#)[References](#)[Tables](#)[Figures](#)[◀](#)[▶](#)[◀](#)[▶](#)[Back](#)[Close](#)[Full Screen / Esc](#)[Printer-friendly Version](#)[Interactive Discussion](#)

Petricoli, A., Ravegnani, F., Giovanelli, G., Bortoli, D., Bonafe, U., Kostadinov, I., and Oulanovsky, A.: Off-axis measurements of atmospheric trace gases by use of an airborne ultraviolet-visible spectrometer, *Appl. Optics*, 41, 5593–5599, doi:10.1364/AO.41.005593, 2002.

5 Platt, U. and Stutz, J.: *Differential Optical Absorption Spectroscopy: Principles and Applications*, Springer Verlag, Heidelberg, 2008.

Prados-Roman, C., Butz, A., Deutschmann, T., Dorf, M., Kritten, L., Minikin, A., Platt, U., Schlager, H., Sihler, H., Theys, N., Van Roozendael, M., Wagner, T., and Pfeilsticker, K.: Airborne DOAS limb measurements of tropospheric trace gas profiles: case studies on the profile retrieval of O₄ and BrO, *Atmos. Meas. Tech.*, 4, 1241–1260, doi:10.5194/amt-4-1241-2011, 2011.

Rodgers, C. D.: *Inverse Methods for Atmospheric Sounding: Theory and Practice*, World Scientific, Singapore, 2000.

15 Rothman, L., Jacquemart, D., Barbe, A., Benner, D., Birk, M., Brown, L., Carleer, M., Chackerian, C., Chance, K., Coudert, L., Dana, V., Devi, V., Flaud, J., Gamache, R., Goldman, A., Hartmann, J., Jucks, K., Maki, A., Mandin, J., Massie, S., Orphal, J., Perrin, A., Rinsland, C., Smith, M., Tennyson, J., Tolchenov, R., Toth, R., Vander Auwera, J., Varanasi, P., and Wagner, G.: The HITRAN 2004 molecular spectroscopic database, *J. Quant. Spectrosc. Ra.*, 96, 139–204, doi:10.1016/j.jqsrt.2004.10.008, 2005.

20 Ryerson, T. B., Andrews, A. E., Angevine, W. M., Bates, T. S., Brock, C. A., Cohen, R. C., Cooper, O. R., de Gouw, J. A., Fehsenfeld, F. C., Ferrare, R. A., Fischer, M. L., Flagan, R. C., Goldstein, A. H., Hair, J. W., Hardesty, R. M., Hostetler, C. A., Jimenez, J. L., Langford, A. O., McCauley, E., McKeen, S. A., Molina, L. T., Nenes, A., Oltmans, S. J., Parrish, D. D., Pederson, J. R., Pierce, R. B., Prather, K., Quinn, P. K., Seinfeld, J. H., Senff, C., Sorooshian, A., Stutz, J., Surratt, J. D., Trainer, M., Volkmer, R., Williams, E. J., and Wofsy, S. C.: The 2010 California Research at the Nexus of Air Quality and Climate Change (CalNex) field study, *J. Geophys. Res.*, in preparation, 2012.

25 Schiller, C., Wahner, A., Platt, U., Dorn, H. P., Callies, J., and Ehhalt, D. H.: Near UV atmospheric absorption-measurements of column abundances during airborne arctic stratospheric expedition, January–February 1989. 2. O₃ Observations, *Geophys. Res. Lett.*, 17, 501–504, doi:10.1029/GL017i004p00501, 1990.

**The CU Airborne
MAX-DOAS
instrument**

S. Baidar et al.

Title Page

Abstract

Introduction

Conclusions

References

Tables

Figures

◀

▶

◀

▶

Back

Close

Full Screen / Esc

Printer-friendly Version

Interactive Discussion



Sinreich, R., Coburn, S., Dix, B., and Volkamer, R.: Ship-based detection of glyoxal over the remote tropical Pacific Ocean, *Atmos. Chem. Phys.*, 10, 11359–11371, doi:10.5194/acp-10-11359-2010, 2010.

Thomson, J., Hayes, P. L., Jimenez, J. L., Adachi, K., Zhang, X., Liu, J., Weber, R. J., and Buseck, R. R.: Aerosol optical properties at Pasadena, CA During CalNex 2010, *Atmos. Environ.*, 55, 190–200, doi:10.1016/j.atmosenv.2012.03.011, 2012.

Trainic, M., Abo Riziq, A., Lavi, A., Flores, J. M., and Rudich, Y.: The optical, physical and chemical properties of the products of glyoxal uptake on ammonium sulfate seed aerosols, *Atmos. Chem. Phys.*, 11, 9697–9707, doi:10.5194/acp-11-9697-2011, 2011.

Vandaele, A., Hermans, C., Simon, P., Carleer, M., Colin, R., Fally, S., Merienne, M., Jenouvrier, A., and Coquart, B.: Measurements of the NO₂ absorption cross-section from 42 000 cm⁻¹ to 10 000 cm⁻¹ (238–1000 nm) at 220 K and 294 K, *J. Quant. Spectrosc. Ra.*, 59, 171–184, doi:10.1016/S0022-4073(97)00168-4, 1998.

Volkamer, R., Spietz, P., Burrows, J., and Platt, U.: High-resolution absorption cross-section of glyoxal in the UV-vis and IR spectral ranges, *J. Photochem. Photobiol. A*, 172, 35–46, doi:10.1016/j.jphotochem.2004.11.011, 2005.

Volkamer, R., Coburn, S., Dix, B., and Sinreich, R.: MAX-DOAS observations from ground, ship, and research aircraft: maximizing signal-to-noise to measure “weak” absorbers, *Proc. SPIE*, 7462, 746203, doi:10.1117/12.826792, 2009a.

Volkamer, R., Ziemann, P. J., and Molina, M. J.: Secondary Organic Aerosol Formation from Acetylene (C₂H₂): seed effect on SOA yields due to organic photochemistry in the aerosol aqueous phase, *Atmos. Chem. Phys.*, 9, 1907–1928, doi:10.5194/acp-9-1907-2009, 2009b.

Wagner, T., von Friedeburg, C., Wenig, M., Otten, C., and Platt, U.: UV-visible observations of atmospheric O₄ absorptions using direct moonlight and zenith-scattered sunlight for clear-sky and cloudy sky conditions, *J. Geophys. Res.*, 107, 4424, doi:10.1029/2001JD001026, 2002.

Wagner, T., Dix, B., von Friedeburg, C., Friess, U., Sanghavi, S., Sinreich, R., and Platt, U.: MAX-DOAS O₄ measurements: a new technique to derive information on atmospheric aerosols – principles and information content, *J. Geophys. Res.*, 109, D22205, doi:10.1029/2004JD004904, 2004.

Wagner, T., Deutschmann, T., and Platt, U.: Determination of aerosol properties from MAX-DOAS observations of the Ring effect, *Atmos. Meas. Tech.*, 2, 495–512, doi:10.5194/amt-2-495-2009, 2009.

**The CU Airborne
MAX-DOAS
instrument**

S. Baidar et al.

[Title Page](#)[Abstract](#)[Introduction](#)[Conclusions](#)[References](#)[Tables](#)[Figures](#)[◀](#)[▶](#)[◀](#)[▶](#)[Back](#)[Close](#)[Full Screen / Esc](#)[Printer-friendly Version](#)[Interactive Discussion](#)

- Wahner, A., Callies, J., Dorn, H. P., Platt, U., and Schiller, C.: Near UV atmospheric absorption-measurements of column abundances during airborne arctic stratospheric expedition, January–February 1989. 1. Technique and NO₂ observations, *Geophys. Res. Lett.*, 17, 497–500, doi:10.1029/GL017i004p00497, 1990a.
- 5 Wahner, A., Callies, J., Dorn, H. P., Platt, U., and Schiller, C.: Near UV atmospheric absorption-measurements of column abundances during airborne arctic stratospheric expedition, January–February 1989. 3. Bro Observations, *Geophys. Res. Lett.*, 17, 517–520, doi:10.1029/GL017i004p00517, 1990b.
- Wang, P., Richter, A., Bruns, M., Rozanov, V. V., Burrows, J. P., Heue, K.-P., Wagner, T.,
10 Pundt, I., and Platt, U.: Measurements of tropospheric NO₂ with an airborne multi-axis DOAS instrument, *Atmos. Chem. Phys.*, 5, 337–343, doi:10.5194/acp-5-337-2005, 2005.
- Wang, P., Richter, A., Bruns, M., Burrows, J. P., Scheele, R., Junkermann, W., Heue, K.-P.,
15 Wagner, T., Platt, U., and Pundt, I.: Airborne multi-axis DOAS measurements of tropospheric SO₂ plumes in the Po-valley, Italy, *Atmos. Chem. Phys.*, 6, 329–338, doi:10.5194/acp-6-329-2006, 2006.
- Wittrock, F., Oetjen, H., Richter, A., Fietkau, S., Medeke, T., Rozanov, A., and Burrows, J. P.:
MAX-DOAS measurements of atmospheric trace gases in Ny-Ålesund – Radiative transfer
studies and their application, *Atmos. Chem. Phys.*, 4, 955–966, doi:10.5194/acp-4-955-2004,
2004.
- 20 Zaveri, R. A., Shaw, W. J., Cziczo, D. J., Schmid, B., Ferrare, R. A., Alexander, M. L.,
Alexandrov, M., Alvarez, R. J., Arnott, W. P., Atkinson, D. B., Baidar, S., Banta, R. M.,
Barnard, J. C., Beranek, J., Berg, L. K., Brechtel, F., Brewer, W. A., Cahill, J. F., Cairns, B.,
Cappa, C. D., Chand, D., China, S., Comstock, J. M., Dubey, M. K., Easter, R. C., Eric-
25 ickson, M. H., Fast, J. D., Floerchinger, C., Flowers, B. A., Fortner, E., Gaffney, J. S.,
Gilles, M. K., Gorkowski, K., Gustafson, W. I., Gyawali, M., Hair, J., Hardesty, R. M., Har-
worth, J. W., Herndon, S., Hiranuma, N., Hostetler, C., Hubbe, J. M., Jayne, J. T., Jeong, H.,
Jobson, B. T., Kassianov, E. I., Kleinman, L. I., Kluzek, C., Knighton, B., Kolesar, K. R.,
Kuang, C., Kubátová, A., Langford, A. O., Laskin, A., Laulainen, N., Marchbanks, R. D.,
30 Mazzoleni, C., Mei, F., Moffet, R. C., Nelson, D., Obland, M. D., Oetjen, H., Onasch, T. B.,
Ortega, I., Ottaviani, M., Pekour, M., Prather, K. A., Radney, J. G., Rogers, R. R., Sand-
berg, S. P., Sedlacek, A., Senff, C. J., Senum, G., Setyan, A., Shilling, J. E., Shrivas-
tava, M., Song, C., Springston, S. R., Subramanian, R., Suski, K., Tomlinson, J., Volk-
amer, R., Wallace, H. W., Wang, J., Weickmann, A. M., Worsnop, D. R., Yu, X.-Y., Zelenyuk, A.,

- and Zhang, Q.: Overview of the 2010 Carbonaceous Aerosols and Radiative Effects Study (CARES), *Atmos. Chem. Phys.*, 12, 7647–7687, doi:10.5194/acp-12-7647-2012, 2012.
- 5 Zieger, P., Weingartner, E., Henzing, J., Moerman, M., de Leeuw, G., Mikkilä, J., Ehn, M., Petäjä, T., Clémer, K., van Roozendaal, M., Yilmaz, S., Frieß, U., Irie, H., Wagner, T., Shaiganfar, R., Beirle, S., Apituley, A., Wilson, K., and Baltensperger, U.: Comparison of ambient aerosol extinction coefficients obtained from in-situ, MAX-DOAS and LIDAR measurements at Cabauw, *Atmos. Chem. Phys.*, 11, 2603–2624, doi:10.5194/acp-11-2603-2011, 2011.

**The CU Airborne
MAX-DOAS
instrument**

S. Baidar et al.

Title Page

Abstract

Introduction

Conclusions

References

Tables

Figures

◀

▶

◀

▶

Back

Close

Full Screen / Esc

Printer-friendly Version

Interactive Discussion



**The CU Airborne
MAX-DOAS
instrument**

S. Baidar et al.

Title Page

Abstract

Introduction

Conclusions

References

Tables

Figures

◀

▶

◀

▶

Back

Close

Full Screen / Esc

Printer-friendly Version

Interactive Discussion

**Table 1.** List of trace gas references used for DOAS analysis.

No.	Molecule	Reference
1	NO ₂ (220 K)	Vandaele et al. (1997)
2	NO ₂ (294 K)	Vandaele et al. (1997)
3	O ₃ (223 K)	Bogumil et al. (2003)
4	O ₃ (243 K)	Bogumil et al. (2003)
5	O ₄ (298 K)	Hermans (2002)
6	CHOCHO (298 K)	Volkamer et al. (2005)
7	HCHO (298 K)	Meller and Moortgat (2000)
8	H ₂ O	Rothman et al. (2005)
9	O ₄	Greenblatt et al. (1990)

The CU Airborne MAX-DOAS instrument

S. Baidar et al.

Table 2. Summary of DOAS analysis settings for different trace gases. 2 Rings (warm and cold) were fitted for HCHO retrievals, and spectra collected for SZA $< \sim 65^\circ$ were only analyzed and hence BrO was not included in the fit.

Trace gas	Wavelength range (nm)	Fitted absorber	Polynomial order
NO ₂	433–460	1, 2, 3, 6, 8, 9	3
CHOCHO	433–460	1, 2, 3, 6, 8, 9	3
HCHO	335–357	1, 2, 3, 4, 5, 7	3
H ₂ O	435–455	1, 2, 4, 5, 6, 8	3
O ₄	350–386	1, 2, 3, 4, 5	3
O ₄	440–490	1, 2, 4, 5, 8	5

[Title Page](#)
[Abstract](#)
[Introduction](#)
[Conclusions](#)
[References](#)
[Tables](#)
[Figures](#)
[Back](#)
[Close](#)
[Full Screen / Esc](#)
[Printer-friendly Version](#)
[Interactive Discussion](#)


The CU Airborne MAX-DOAS instrument

S. Baidar et al.

Table 3. Detection limits of CU AMAX-DOAS instrument in the clean free troposphere and the boundary layer in polluted urban conditions like SCAB for different integration times.

Trace gas	Free troposphere (FT) (ppt)		Boundary layer (BL) (ppt)	
	30 s	2 s	30 s	2 s
NO ₂	5	30	30	120
CHOCHO	3	16	16	65
HCHO	98	290	540	1355
$\epsilon_{477\text{nm}}$	0.002	0.002	0.006	0.006
$\epsilon_{360\text{nm}}$	0.004	0.004	0.012	0.012

[Title Page](#)
[Abstract](#)
[Introduction](#)
[Conclusions](#)
[References](#)
[Tables](#)
[Figures](#)
[Back](#)
[Close](#)
[Full Screen / Esc](#)
[Printer-friendly Version](#)
[Interactive Discussion](#)


The CU Airborne MAX-DOAS instrument

S. Baidar et al.

Table 4. Relative error of geometric approximation compared to AMF calculated at 455 nm using radiative transfer program McArtim under different scenarios.

Altitude (km)	Solar zenith angle (SZA)	Most probable conditions	Boundary layer height (m)		NO ₂ concentration (ppb)		Surface albedo (SA)		Single scattering albedo (SSA)		Aerosol optical depth (AOD)	
			500	1500	5	20	0.05	0.15	0.90	0.99	0.10	0.80
2 (low)	20	6.3	3.3	9.0	7.2	5.6	3.0	12.2	4.4	9.6	4.3	6.7
	40	4.7	1.0	5.6	5.1	3.2	5.7	9.4	1.1	6.9	2.9	2.6
	60	5.9	7.3	6.3	6.0	7.0	15.3	0.7	8.0	3.3	3.4	11.0
3.5 (high)	20	3.0	6.3	0.3	2.8	3.2	15.2	5.3	5.3	0.30	4.6	1.0
	40	5.4	8.6	3.1	4.1	5.1	15.9	2.8	7.6	2.1	6.9	4.9
	60	16.1	16.4	14.0	14.5	16.5	25.0	8.3	17.5	11.6	14.2	19.3

[Title Page](#)
[Abstract](#)
[Introduction](#)
[Conclusions](#)
[References](#)
[Tables](#)
[Figures](#)
[Back](#)
[Close](#)
[Full Screen / Esc](#)
[Printer-friendly Version](#)
[Interactive Discussion](#)


The CU Airborne MAX-DOAS instrument

S. Baidar et al.

Table 5. Uncertainty in aerosol extinction coefficient due to uncertainty in model input parameters.

Parameter	Uncertainty in parameter	Uncertainty in extinction coefficient
Surface albedo	± 0.05	< 2 %
Single scattering albedo	± 0.05	< 2 %
Asymmetry parameter	± 0.07	Up to 10 %
Temperature	$\pm 5^\circ\text{C}$	Up to 10 %
Pointing accuracy	$\pm 0.35^\circ$	Mostly in transition layer

[Title Page](#)
[Abstract](#)
[Introduction](#)
[Conclusions](#)
[References](#)
[Tables](#)
[Figures](#)
[◀](#)
[▶](#)
[◀](#)
[▶](#)
[Back](#)
[Close](#)
[Full Screen / Esc](#)
[Printer-friendly Version](#)
[Interactive Discussion](#)


The CU Airborne MAX-DOAS instrument

S. Baidar et al.

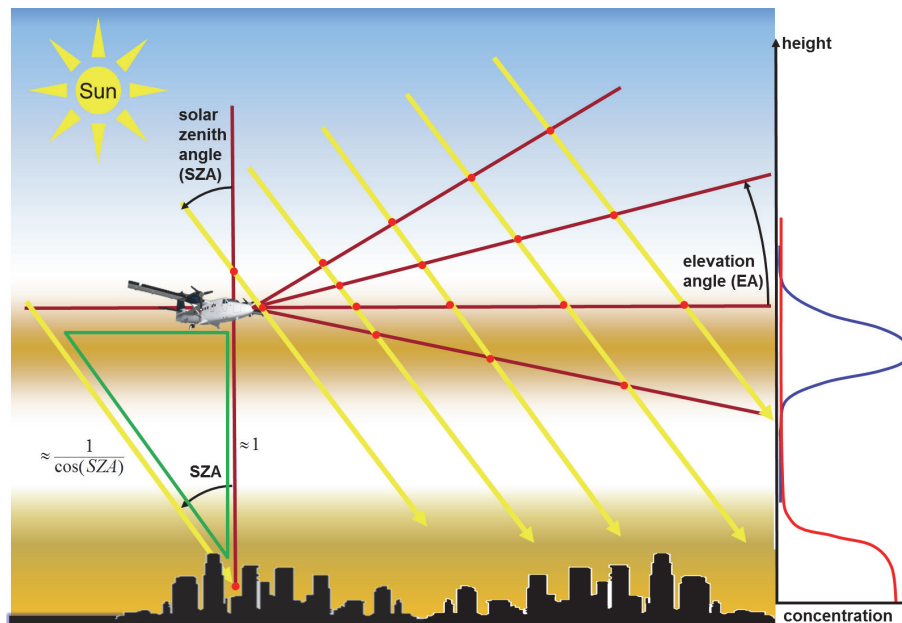


Fig. 1. Schematic of the AMAX-DOAS measurement principle. Individual EAs contain different amount of information from different layers in the atmosphere. The inset (green triangle) illustrates the geometric approximation used to convert nadir dSCDs to VCDs.

Title Page

Abstract

Introduction

Conclusions

References

Tables

Figures

◀

▶

◀

▶

Back

Close

Full Screen / Esc

Printer-friendly Version

Interactive Discussion



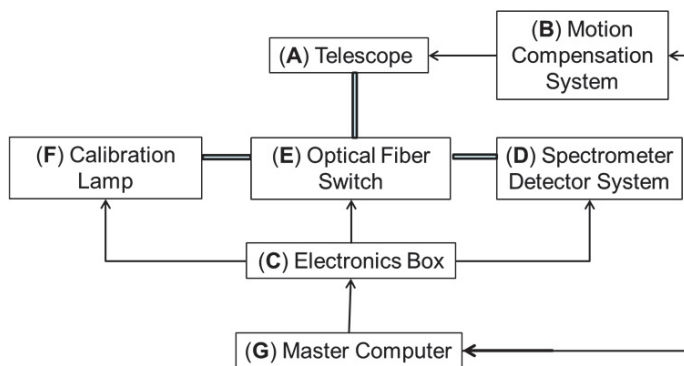
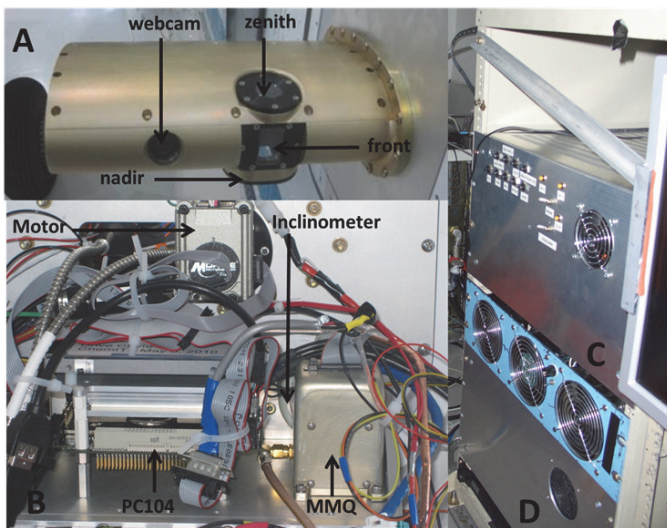


Fig. 2. CU AMAX-DOAS instrument setup aboard the NOAA Twin Otter during the CalNex and CARES campaigns.

**The CU Airborne
MAX-DOAS
instrument**

S. Baidar et al.

Title Page

Abstract Introduction

Conclusions References

Tables Figures

◀ ▶

◀ ▶

Back Close

Full Screen / Esc

Printer-friendly Version

Interactive Discussion



The CU Airborne MAX-DOAS instrument

S. Baidar et al.

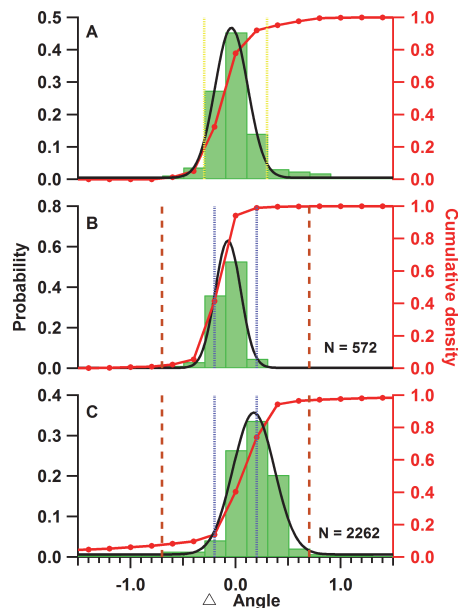


Fig. 3. (A) Distribution of difference in pitch angle of the aircraft measured at real time by the MMQ-G angle sensor of the CU-AMAX-DOAS and aircraft avionics system of NSF/NCAR GV HIAPER aircraft during a research flight on 24 February 2012. 1σ angle accuracy (0.29°) of the MMQ-G sensor is shown in yellow dotted lines. 1σ for the Gaussian fit (black line) is 0.16° . Distribution of elevation angle accuracy of the CU AMAX-DOAS telescope (B) from the above mentioned flight on NSF/NCAR GV HIAPER flight, (C) during RF#46 aboard NOAA Twin Otter on 16 July 2010. 1σ for the Gaussian fits (black lines) are 0.12° and 0.2° for instrument aboard HIAPER and Twin Otter aircraft respectively and are within the resolution of the motor internal encoder (0.2°), shown in blue dotted lines. Brown dashed lines represent the motor tolerance level (0.7°) set in the software before an automatic reset of the motor position takes place. The red lines represent the cumulative densities.

[Title Page](#)
[Abstract](#)
[Introduction](#)
[Conclusions](#)
[References](#)
[Tables](#)
[Figures](#)
[Back](#)
[Close](#)
[Full Screen / Esc](#)
[Printer-friendly Version](#)
[Interactive Discussion](#)


The CU Airborne
MAX-DOAS
instrument

S. Baidar et al.

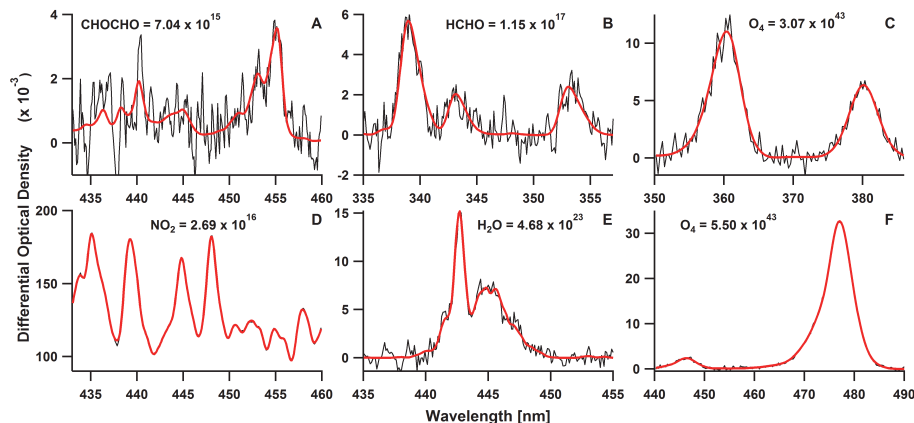


Fig. 4. Spectral proofs for the detection of: **(A)** CHOCHO, **(B)** HCHO, **(C)** O₄ at 360 nm, **(D)** NO₂, **(E)** H₂O and **(F)** O₄ at 477 nm. CHOCHO and NO₂ fits are from 14 July 2010 at 22:08 UTC at ~ 150 m AGL. HCHO and H₂O fits are from 16 July 2010 at 20:19 UTC at ~ 600 m AGL. O₄ fits are from the same flight at 20:11 UTC at ~ 3000 m AGL. The black lines represent the measured spectra and red lines are fitted reference cross sections. Note that for NO₂ and O₄ at 477 nm, the absorptions are so strong that the black lines are not visible. All the fits are for 0° EA.

[Title Page](#)[Abstract](#)[Introduction](#)[Conclusions](#)[References](#)[Tables](#)[Figures](#)[◀](#)[▶](#)[◀](#)[▶](#)[Back](#)[Close](#)[Full Screen / Esc](#)[Printer-friendly Version](#)[Interactive Discussion](#)

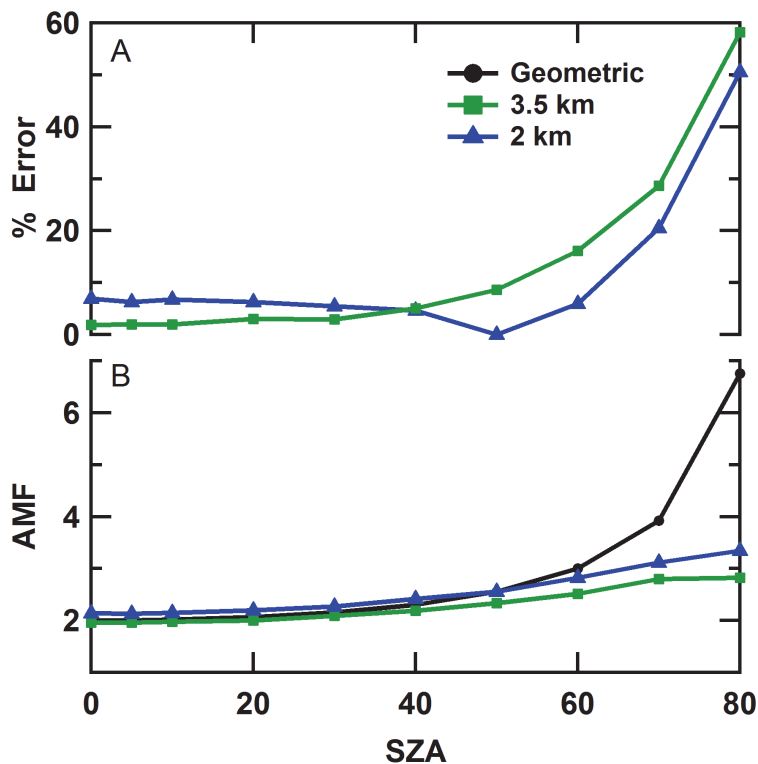


Fig. 5. (A) Relative error of geometric air mass factor (geoAMF) compared to AMF calculated using RTM, McArtim for flight altitude of 3.5 km (green) and 2 km (blue) AGL, for most likely atmospheric conditions in South Coast Air Basin (SCAB). **(B)** AMF calculated using McArtim (green and blue) and geoAMF (black). Most likely atmospheric state in SCAB: surface albedo = 0.10, single scattering albedo = 0.94, g parameter = 0.68, aerosol optical depth = 0.4, boundary layer height = 1 km and NO₂ mixing ratio = 10.0 ppb.

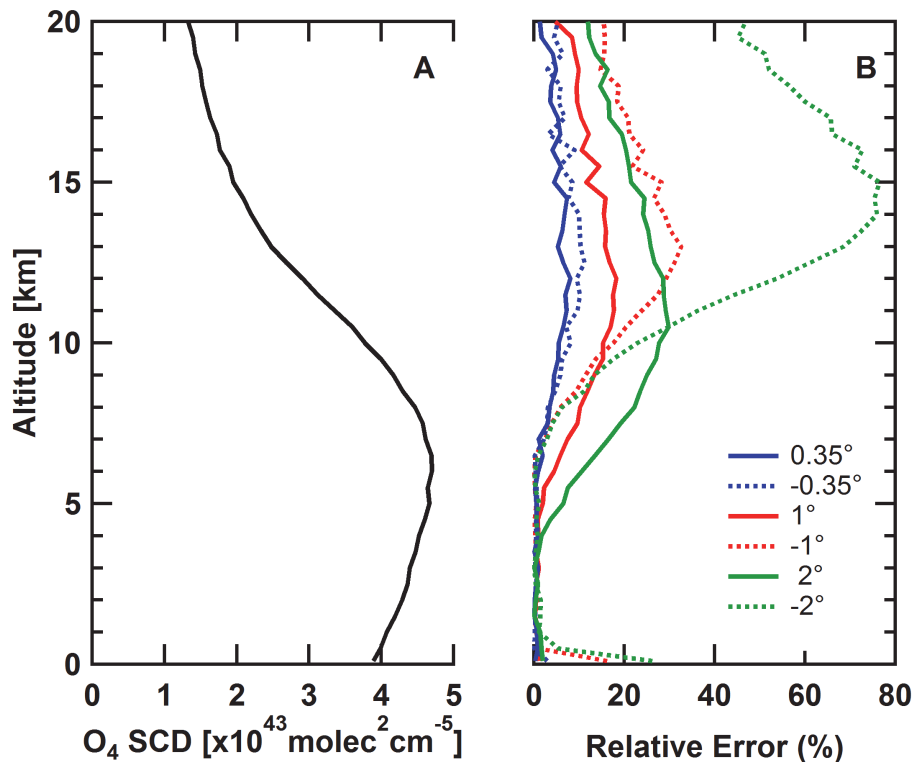


Fig. 6. (A) Vertical profile of O₄ SCDs calculated for 0° EA at 477nm using McArtim (US standard atmosphere with exponential aerosol extinction profile with extinction of 0.2 km⁻¹ at the ground and 2.5 km scale height). **(B)** Relative error in O₄ SCDs for 0.35° (blue), 1° (red) and 2° (green) pointing error of the telescope at 0° EA. The solid and dashed lines represent angles above and below the horizon, respectively.

The CU Airborne MAX-DOAS instrument

S. Baidar et al.

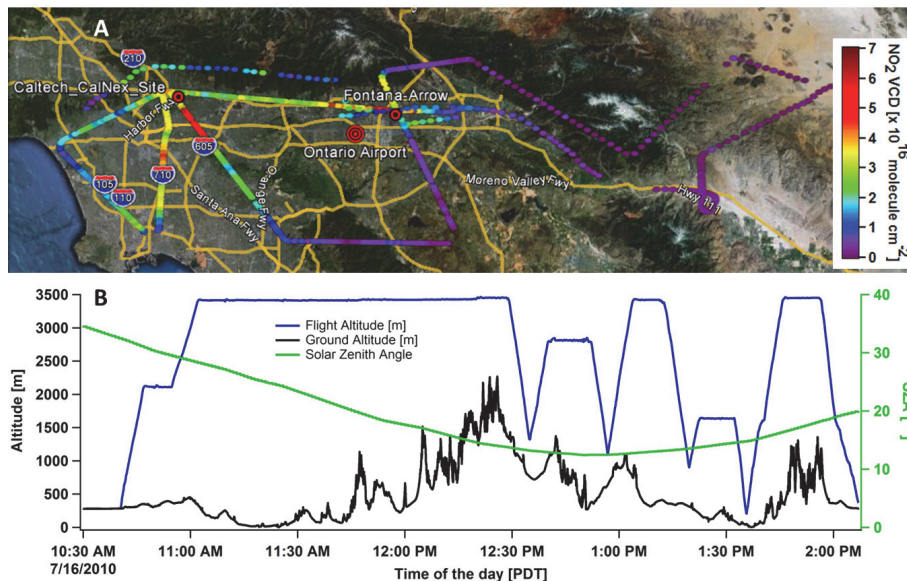


Fig. 7. (A) Map showing horizontal distribution of NO_2 VCDs below the aircraft from RF#46 on 16 July 2010 (10:30–14:10 Pacific Daylight Time, PDT) in the SCAB. GMAX-DOAS instruments deployment sites and the base airport for the Twin Otter are shown as red targets. **(B)** Time trace of flight altitude (blue), ground altitude (black) and SZA (green) from the same flight.

Title Page

Abstract

Introduction

Conclusions

References

Tables

Figures

◀

▶

◀

▶

Back

Close

Full Screen / Esc

Printer-friendly Version

Interactive Discussion



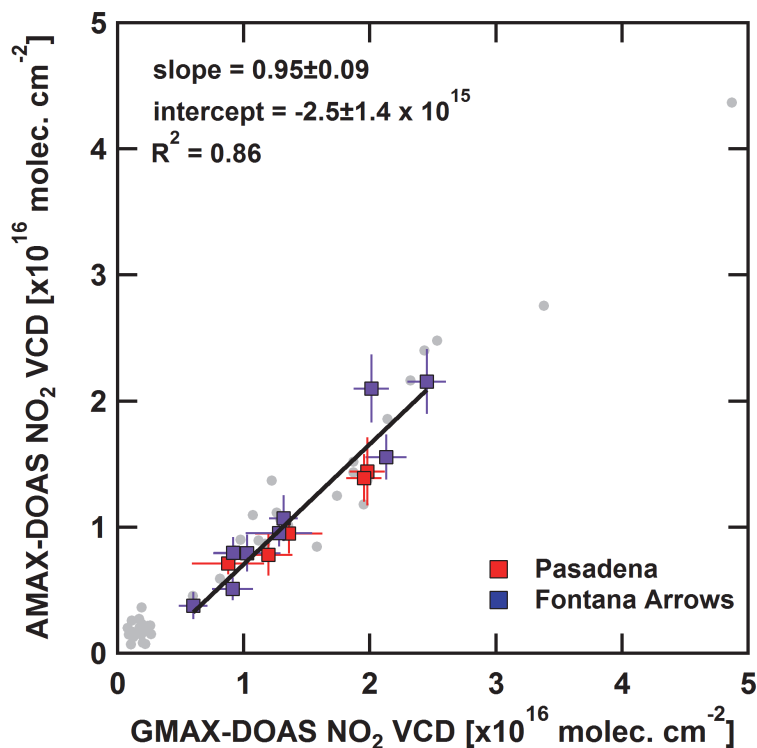


Fig. 8. Correlation plot of NO_2 VCDs between CU AMAX-DOAS and two GMAX-DOAS instruments deployed in California during the CalNex and CARES field campaigns. Grey dots represent all data from both CalNex and CARES campaigns (see text for filtering conditions). Data from CalNex further constrained for relative azimuth between plane heading and GMAX-DOAS viewing geometry $< \pm 15^\circ$ and NO_2 VCD variability $< 8 \times 10^{15}$ molecules cm^{-2} are shown in red and blue. Black line is the linear fit through the colored points.

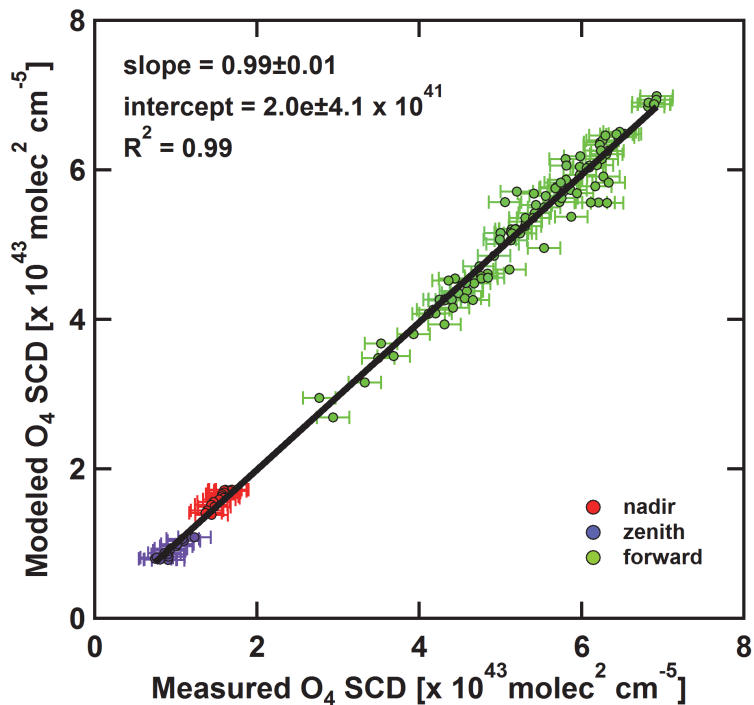


Fig. 9. Correlation plot of modeled and measured O_4 SCDs at 477 nm for the case study shown in Fig 10b. SCD of the zenith reference (9×10^{42} molecules 2 cm $^{-5}$) has been added to the measured O_4 dSCDs. Forward viewing geometry includes 0° , $\pm 2^\circ$, $\pm 5^\circ$ EAs.

**The CU Airborne
MAX-DOAS
instrument**

S. Baidar et al.

Title Page

Abstract

Introduction

Conclusions

References

Tables

Figures

⏪

⏩

◀

▶

Back

Close

Full Screen / Esc

Printer-friendly Version

Interactive Discussion



The CU Airborne
MAX-DOAS
instrument

S. Baidar et al.

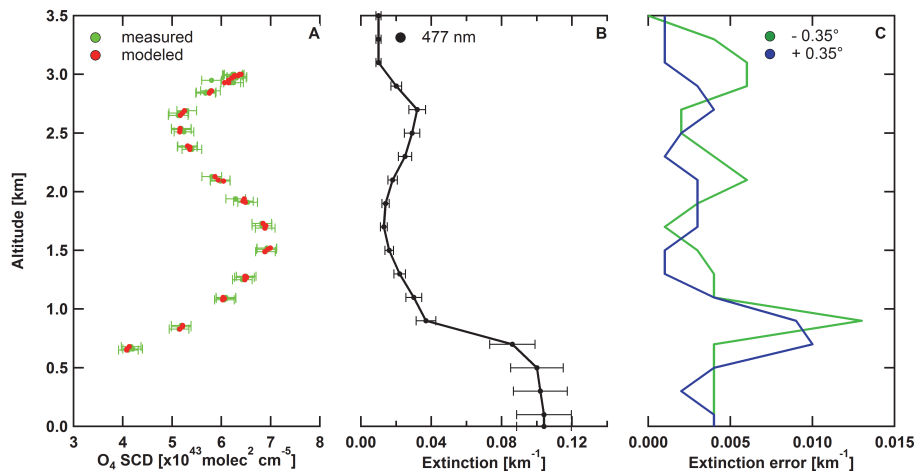


Fig. 10. (A) Measured (green) and simulated (red) vertical profiles of O₄ SCDs for EA 0° at 477 nm from a low approach at Brackett airfield during RF#46 on 16 July 2010 in SCAB. (B) Corresponding aerosol extinction vertical profile retrieved at 477 nm. (C) Error contribution in extinction due to angle uncertainty of $\pm 0.35^\circ$. Note that the aircraft only flew down to ~ 600 m AGL during the low approach and a set of downward EAs at that altitude was used to probe the lower altitudes.

The CU Airborne MAX-DOAS instrument

S. Baidar et al.

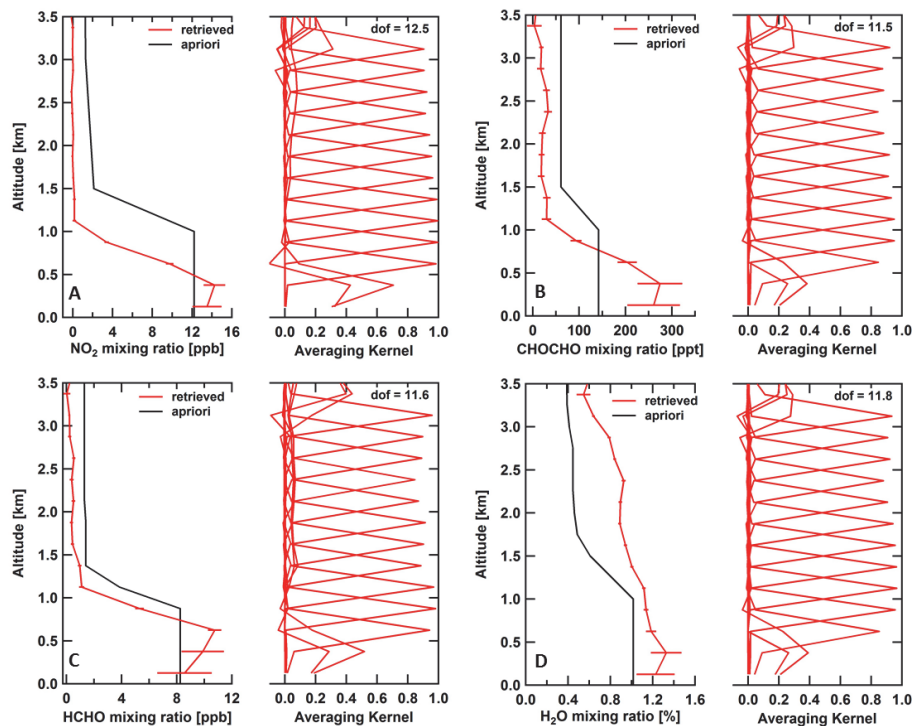


Fig. 11. Retrieved vertical profiles and corresponding averaging kernels for **(A)** NO_2 , **(B)** CHOCHO, **(C)** HCHO and **(D)** H_2O from the low approach at Brackett airfield. NO_2 , CHOCHO and HCHO profiles show most of the trace gases are located close to the source region inside the BL. Averaging kernels indicate almost constant sensitivity for all trace gases over the entire altitude range.

[Title Page](#)
[Abstract](#)
[Introduction](#)
[Conclusions](#)
[References](#)
[Tables](#)
[Figures](#)
[Back](#)
[Close](#)
[Full Screen / Esc](#)
[Printer-friendly Version](#)
[Interactive Discussion](#)
